東京大学 大学院新領域創成科学研究科
基盤科学研究系
先端エネルギー工学専攻

平成 22 年度

修士論文

Auto-tracking Phased Array System for Wireless Power Supply to

Micro Aerial Vehicles

－ MAV へのマイクロ波自動追尾電力供給システム －

2011 年 2 月提出
指導教員　小紫　公也　教授

096062　小田　章徳

Acknowledgements

Contents

Chapter 4.   Receiving system

Chapter 5.   System integration and Demonstration

Chapter 6.   Conclusions

Reference

List of Figures

Chapter 1.　Introduction

Chapter 2.　Transmitting system

Chapter 3. Tracking system

Chapter 4. Receiving system

Chapter 5.   System integration and Demonstration

List of Tables

Chapter 1. Introduction

1.1. Objective of our research

Today, several kinds of transportation systems, such as automobiles and aircrafts, have already been available. These transportation systems are realized by fossil fuels which can generate a lot of energy in small amounts and high mobility and long traveling come to fruition. But, in terms of reducing carbon dioxide, new power sources without fossil fuel are required, for example electric battery. Though, it is difficult to substitute gasoline with electric battery because of its smallness of electrical capacity, large usage of material resource, and lowered system efficiency that is caused by its heaviness. To reduce the battery weight, battery charging while the vehicle is moving or frequent power feeding at energy stations is needed, so WPT (wireless power transmission) is very important and key technology.

Existing micro robots which are used for surveillance of hazard areas and for medical checkup are so small that it cannot move, if they are connected by a wire cable with an external power supply, because of the cable weight. If their power sources become batteries, operating time, size, and movable area of them are not unboundedly [1]. Recently, with development of low power (about mW level) IC, sensor, and LED, more enhanced and powerful devices are designed and new application are expected.

The objective of this study is to develop a wireless power supply system to a moving object and our laboratory suggests the WPT system to MAVs (Micro Aerial Vehicles).
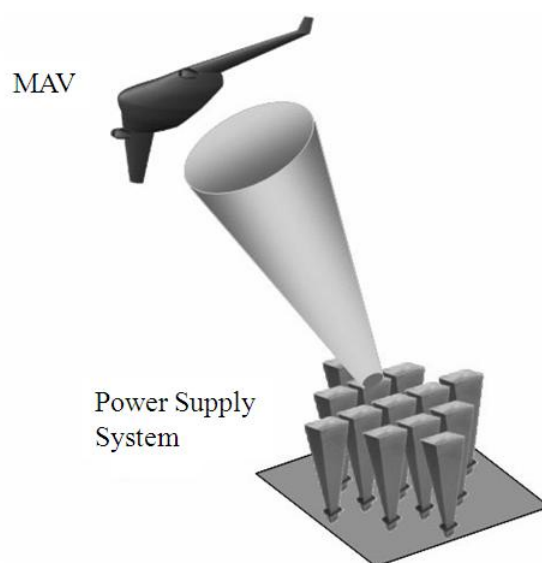
Figure1.1 Concept of WPT to MAV

1.2. Previous studies about WPT

WPT technologies have are studied at many research institutes until now, varieties of WPT method were suggested and several of them were already realized. For example, EI (Electromagnetic Induction) method which is used for *SUICA*, MR (Magnetic Resonance) method which is suggested by MIT at 2007 [2], and MWPT (Microwave Wireless Power Transmission) method and LET (Laser Energy Transmission) method that are represented as SPS (Solar Power Satellite) [3]. These technologies should be creatively used with consideration of size and weight of transmission and receiving antennas, amount of transmission power, existence or non-existence of obstructions on pathways. Figure1.2 shows relationship between transmission power and transmission distance and Table1.1 shows relationship between transmission distance and system size of each WPT method. As you can see this figure and table, MWPT method has the capability of low power and long distance of transmission and allows compactness of its system, mainly receiving antenna size, so MWPT method is suitable for wireless power supply to MAVs.
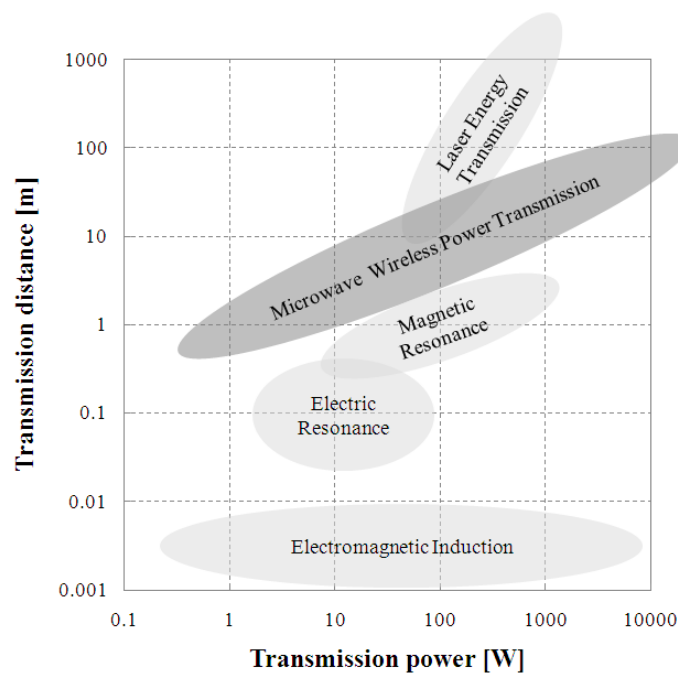
Figure1.2 Relation between power and distance of WTP

Table1.1 Transmission range of WTP

Method	Relation between transmission distance and system size
Magnetic Induction	$L/D < 1$
Magnetic Resonance	$1 < L/D < 10$
Microwave Wireless Power Transmission	$L/D \ll 10$
Laser Energy Transmission	

L : Transmission distance
D : Coil diameter or transmitter aperture

1.3. History and past studies of MPWT

Wireless Power Transmission using electromagnetic wave has been suggested since early twentieth century, Nicola Tesla did a first experiment of it. To substantiate the theory that is "electromagnetic wave is energy" this idea comes from Maxwell equation, he tried a WPT experiment using 150kHz, 300kW electromagnetic wave, but his challenge was unsuccessful [4]. It was because 150 kHz electromagnetic wave does not have capability of power deposition at a point, so power density of electromagnetic field near a receiving antenna was attenuated as low as telecommunication waves. On theoretical grounds, large antenna aperture plane and higher frequency are required to concentrate electromagnetic wave.

In the 1960's, since microwave technology was developed and high gain antenna appeared, microwave beam could be formed and Dr. William Brown succeed their various experiments about verification of MWPT [5]. In the 1975, the largest MWPT experimental test in the world was conducted by Dr. Brown at the Goldstone of The United States. The experimental condition was;

Transmitting system	:	450kW CW klystron
Frequency	:	2.388GHz
Transmitting antenna	:	26ϕ Cassegrain parabola antenna
Transmission distance	:	1.54km
Receiving system (rectenna)	:	$3.4 \times 7.2\text{m} = 24.5\text{m}^2$
Receiving power	:	30kW DC (RF-DC conversion efficiency 82.5%)
Total efficiency	:	6.7% (30kW/450kW)

Around the same time, Dr. Brown recorded DC-RF-DC conversion efficiency 54% at 495W DC using magnetrons and horn antennas at his laboratory. Microwave could be created effectively by using electron tubes like magnetron and frequency could be high enough to fabricate theoretical size antennas at this time. Therefore, wireless power transmission had been called "microwave power transmission" and studied it.

Since 1980's, Japan became a leading country of MWPT and has been developed researches about SPS. SPS which was suggested in 1968 was a most suitable and largest application of MWPT and became a main research topic. Envisaged frequency of SPS is IMS band like 2.45GHz and 5.8GHz.

1.4. Concept of our MWPT system

The concept of our MWPT system is as follows. An MAV, working over the hazard area struck by disaster for example, comes back to the power station when its battery becomes low. Then the battery is charged by receiving the microwave beam transmitted from the power station while it is circling over it. As a result, the MAV battery is charged semi-automatically without landings and take-offs. Figure1.3 shows the schematic of the system developed in our laboratory [6].

The Microwave power supply system consists of three subsystems; power transmitting, receiving (rectenna), and tracking subsystem. In the transmitting subsystem, a microwave beam of 5.8GHz is formed and steered using an active phased array antenna. In the receiving system, the microwave power received by an antenna is converted to DC power by an in-house rectifier and used to drive an electric motor on the MAV model. In the tracking system, the position of the MAV is detected by using 2.45GHz microwave at a pilot signal from the MAV and, a software-retro-directive mechanism is adopted.

The microwave beam from the transmitting system is pointed to the MAV using the information of its position analyzed in the tracking system and the MAV flies by the electric motor on it using the power received by the receiving system.
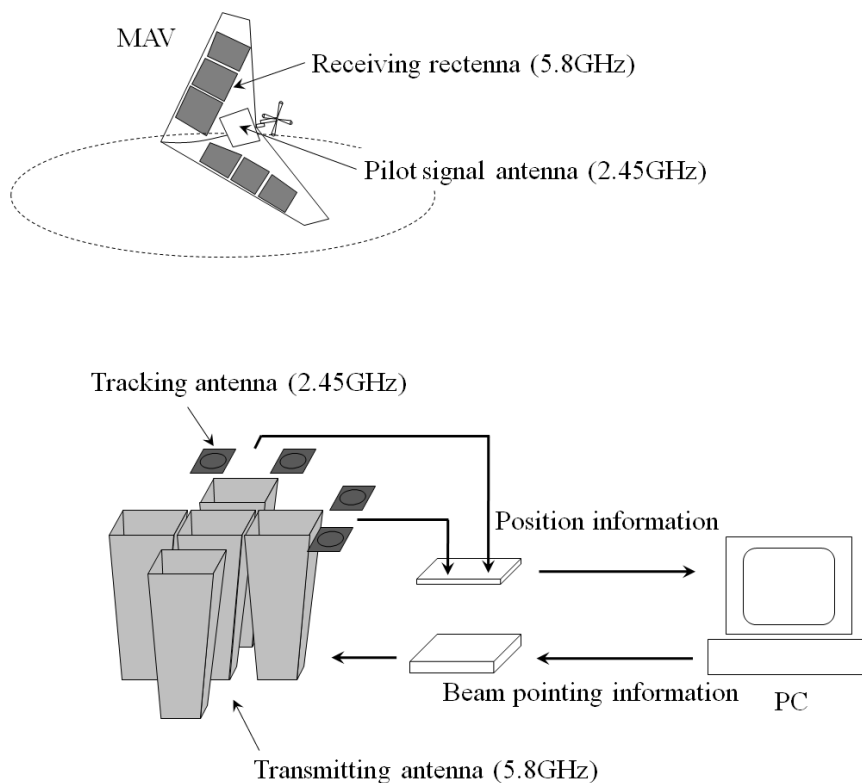
Figure1.3 Overview of our MWPT system

Chapter 2. Transmitting system

2.1. System overview

At the transmitting system, 5.8GHz microwave was used and the phased array function was adopted. The active phased array system can steer a microwave beam not mechanically but electrically, so it is realized to point a microwave beam toward the target which move quickly.

2.2. Theory of transmitting system

In this section, a basic theory of the phased array which was adopted as the transmitting system is introduced. At the phased array system, synchronizing phases is a key point to get a high efficiency microwave beam.

First, for simplicity, if there are two point wave sources with spacing d, which are in the coordinate phase, electromagnetic field radiated from one point wave source is

$$E = E_0 \exp(kr) \tag{2.1}$$

Here k is the free-space wave number.

$$k = 2\pi/\lambda \tag{2.2}$$

And then the composite electromagnetic field radiated from these two point wave sources are expressed as

$$E_{\mathrm{com}} = E_1 \exp(ikr_1) + E_2 \exp(ikr_2) \tag{2.3}$$

The condition for maximizing this composite field amplitude is given by

$$k(r_1 - r_2) = 2n\pi \tag{2.4}$$

Assuming that the field is sufficiently far from the two point wave sources as Figure2.1 show, it is approximated with the spacing d and angle α with the vertical axis in the following form

$$kd \sin \alpha = 2n\pi \tag{2.5}$$

Or, replacing $k = 2\pi/\lambda$, Equation(2.5) is rewritten as follows

$$d \sin \alpha = n\lambda \tag{2.6}$$

Now if the wave source phase is shifted by θ against the other wave source, the amplitude of the composite electromagnetic field is

$$E_{\mathrm{com}} = E_1 \exp(ikr_1) + E_2 \exp(i(kr_2 + \theta)) \tag{2.7}$$

The maximizing condition is similar to the case of above

$$kd \sin \alpha = 2n\pi + \theta \tag{2.8}$$

In order to maximizing the electromagnetic field at an angle α with the vertical axis, setting $n = 0$, the phase to shift is expressed as following form

$$\theta = kd \sin \alpha \tag{2.9}$$

Taking into account that θ varies from $-\pi$ to π, Equation(2.9) becomes

$$-\arcsin(\lambda/2d) \le \alpha \le \arcsin(\lambda/2d) \tag{2.10}$$

In this way the steering angle interval can be determined from the wave length λ and the antenna spacing d.
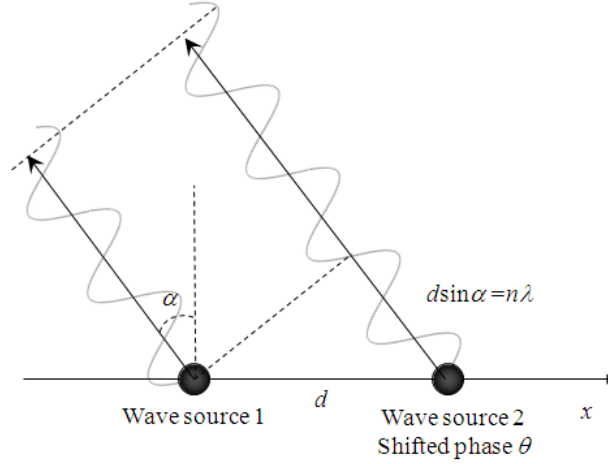
Figure2.1 Simple model of two wave source

2.3. Radiated electromagnetic field from the horn antenna

Let be the electric flux density D, magnetic flux density B, electric field E, magnetic filed H, Maxwell's equations are written as

$$\text{div}D = \rho \qquad \text{div}B = 0$$

$$\text{rot}H - \frac{\partial D}{\partial t} = i \qquad \text{rot}E + \frac{\partial B}{\partial t} = 0 \tag{2.11}$$

Here with the permittivity ε, permeability μ and electric conductivity σ, there are following relations.

$$D = \varepsilon E \quad , \quad B = \mu H \quad , \quad i = \sigma E \tag{2.12}$$

With the angular frequency ω, Equation(2.11) can be expressed in the components

$$(\nabla^2 + \omega^2 \varepsilon\mu - j\omega\mu\sigma)E_i = 0$$

$$(\nabla^2 + \omega^2 \varepsilon\mu - j\omega\mu\sigma)H_i = 0 \qquad i = x, y, z \tag{2.13}$$

Here γ is the cutoff wavenumber

$$\gamma = \sqrt{\omega^2 \varepsilon\mu - j\omega\mu\sigma} \tag{2.14}$$

In rectangular waveguides, the condition and boundary conditions are

$$\sigma = 0$$

$$E_y = 0 \quad \text{at } x = \pm\frac{a}{2} \qquad , \qquad E_x = 0 \quad \text{at } y = \pm\frac{b}{2} \tag{2.15}$$

6
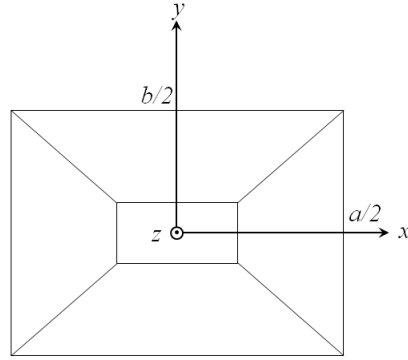
Figure2.2 Aperture of rectangular waveguide

Assuming the propagation fields along the guide direction

$$\boldsymbol{E} = \boldsymbol{E}(x,y)e^{j\omega t - \beta z} \quad , \quad \boldsymbol{H} = \boldsymbol{H}(x,y)e^{j\omega t - \beta z} \tag{2.16}$$

Here β is the propagation wavenumber along the guiding direction. Then the each field component is given by

$$E_x = -\frac{j\omega\mu}{\beta^2 + \omega^2 \varepsilon\mu} \frac{n\pi}{b} H_0 \sin\left(\frac{2m\pi}{a}x\right) \cdot \cos\left(\frac{2n\pi}{b}y\right) \cdot e^{j\omega t - \beta z}$$

$$E_y = \frac{j\omega\mu}{\beta^2 + \omega^2 \varepsilon\mu} \frac{m\pi}{a} H_0 \cos\left(\frac{2m\pi}{a}x\right) \cdot \sin\left(\frac{2n\pi}{b}y\right) \cdot e^{j\omega t - \beta z}$$

$$E_z = 0$$

$$H_x = -\frac{\beta^2}{\beta^2 + \omega^2 \varepsilon\mu} \frac{2m\pi}{a} H_0 \cos\left(\frac{2m\pi}{a}x\right) \cdot \sin\left(\frac{2n\pi}{b}y\right) \cdot e^{j\omega t - \beta z}$$

$$H_y = -\frac{j\omega\mu}{\beta^2 + \omega^2 \varepsilon\mu} \frac{2n\pi}{b} H_0 \sin\left(\frac{2m\pi}{a}x\right) \cdot \cos\left(\frac{2n\pi}{b}y\right) \cdot e^{j\omega t - \beta z}$$

$$H_z = H_0 \sin\left(\frac{2m\pi}{a}x\right) \cdot \sin\left(\frac{2n\pi}{b}y\right) \cdot e^{j\omega t - \beta z} \tag{2.17}$$

In this experiment, the parameters are as shown Table2.1.

Table2.1 Parameters of horn antenna and electromagnetic field

Parameters	f [Hz]	ω [rad/s]	ε [F/m]	μ [H/m]	a [m]	b [m]
Value	5.8×10^9	3.64×10^{10}	8.84×10^{-12}	1.26×10^{-6}	0.04	0.02

7

So, the number of m, n are decided to

$$m = 1 \ , \ n = 0 \tag{2.18}$$

And thus, we obtain the following propagation fields

$$E_y = E_0 \cos\left(\frac{\pi}{a}x\right) \cdot e^{j\omega t - \beta z} \qquad H_x = -\frac{\gamma}{j\omega\mu} E_0 \cos\left(\frac{\pi}{a}x\right) \cdot e^{j\omega t - \beta z}$$

$$H_z = -H_0 \sin\left(\frac{\pi}{a}x\right) \cdot e^{j\omega t - \beta z} \qquad E_x = E_z = H_y = 0 \tag{2.19}$$

This field is found to be constant along the y-direction and have only the y-component. So, there are no needs to consider the x and z components.

Because of the plane waves in wave guides change to spherical waves in radiating to the free space, there is a need for taking the path difference into account to consider the radiation fields in the aperture plane. Setting the base length to the path length along the z-axis, the path difference is written as

$$\delta_{\text{sph}} = \frac{\pi l}{\lambda}\left(\left(\frac{x}{l_a}\right)^2 + \left(\frac{y}{l_b}\right)^2\right) \tag{2.20}$$
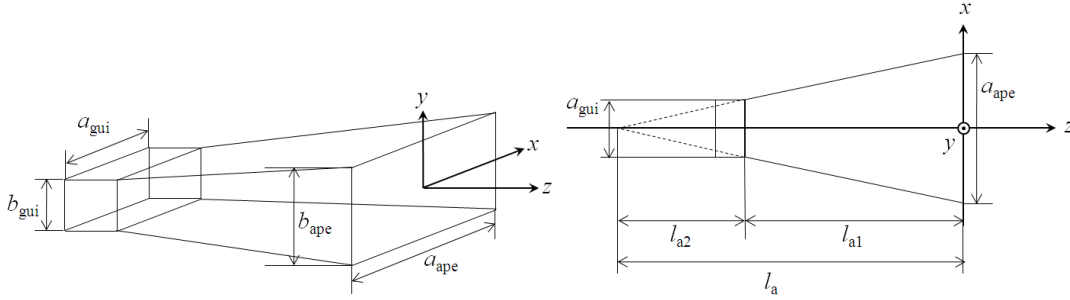
Figure2.3 Dimensions of horn antenna

Assuming the electric field at the center in the aperture plane is E_{oy}, the y-component of the electric field is

$$E_y = E_{0y} \cos\left(\frac{\pi}{a_2}x\right) \cdot \exp(-j\delta_{\text{sph}}) \tag{2.21}$$

Next regarding the electromagnetic field propagating toward the positive z-direction as the radiation field from the set of electric and magnetic unit currents, the combined field becomes

$$E_{ay} = -\xi \frac{E_y}{4\pi} \frac{j\beta}{r}(\cos\alpha_x + \cos\alpha_y) \cdot \exp(-j\beta\gamma)$$

$$H_{ax} = E_{ay}/\eta$$

$$E_r = E_{ax} = H_r = H_{ay} = 0 \tag{2.22}$$

Thus the radiation field from the horn antenna are obtained by Equation(2.22).

$$E_{ay} = \xi \frac{j\beta E_{0y}}{4\pi} \cdot \frac{\exp(-j\beta\gamma)}{r} (\cos\alpha_x + \cos\alpha_y) \int_{-\frac{a}{2}}^{\frac{a}{2}} dx \int_{-\frac{b}{2}}^{\frac{b}{2}} dy \cos\left(\frac{\pi}{a_2}x\right) \exp(-j\delta)$$

$$H_{ax} = E_{ay}/\eta$$

$$E_r = E_{ax} = H_r = H_{ay} = 0 \tag{2.23}$$

2.4. Experimental setup of transmitting system

Figure2.4 shows the diagram of the transmitting system. Firstly a microwave from a 5.8GHz oscillator are amplified and divided into five lines. Because of the divider has eight output ports, the No.5 to No.8 are terminated and used only the other five ports. And then four 6-bit digital phase shifters change the each microwave phase but these phase shifters have insertion losses, so the microwaves are amplified by two steps. The driver amplifier amplified the power which significantly decreased by the phase shifters' insertion losses. Next the power amplifier amplified to the necessity power level, that is, from several mW to about 1W.

Figure2.5 shows two-dimensional antenna array. The two-dimensional antenna array is composed of five horn antennas which arranged crosswise on the x-axis and y-axis. The horn antenna spacing *d* was set to 110 mm.
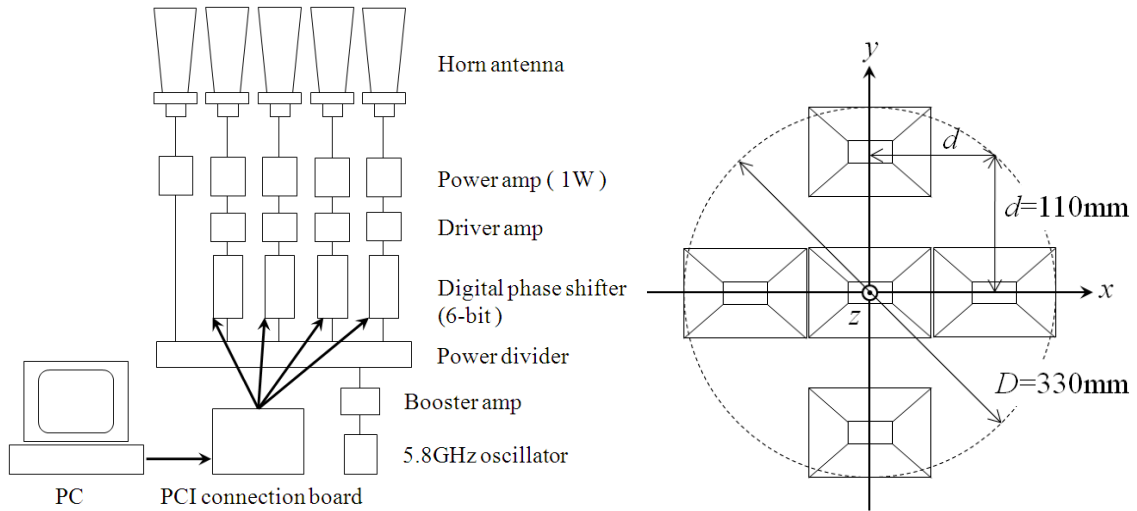
Figure2.4 Diagram of the transmitting system (Left)

Figure2.5 Two-dimensional transmitting antenna array (Right)

2.5. Experimental devices of transmitting system

2.5.1. 5.8GHz oscillator

Figure2.6 shows the 5.8GHz oscillator "ArumoTech - OS00T2182". This oscillator is composed of plate-tuning method and Metal Oxide Semiconductor Field Effect Transistor (MOSFET). The Output connector shape is SMA-J and operating voltage is DC+12V. The output power is stable and about 10dBm.

2.5.2. Booster amp

Figure2.7 shows the booster amplifier "ArumoTech - AP00T2388". The input and output connector shape is SMA-J and operating voltage is DC+12V. The gain of this amplifier is 4.5 dB. Without this booster amplifier, the final output power often fluctuates due to the changing power loss by the phase shifters. Then this amplifier boosted the power level before the divider and saturated it after the power amplifiers. Consequently this booster amplifier can stabilize the final output power level.
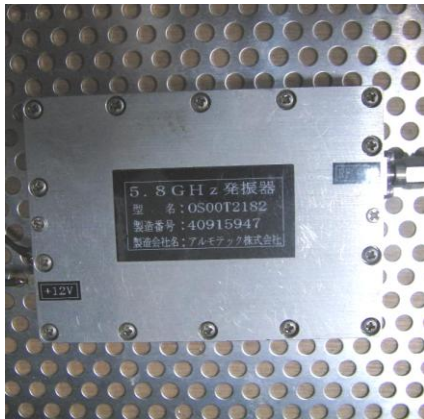
Figure2.6 Picture of 5.8GHz oscillator (Left)
Figure2.7 Picture of booster amplifier (Right)
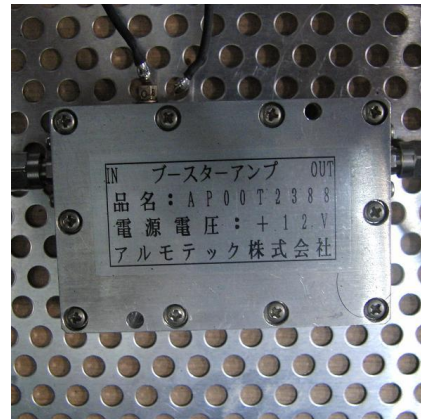
2.5.3. Power divider

Figure2.8 shows the 8-ways power divider "ArumoTech - PD00T2301". At this power divider, the microwave from the booster amp is divided into five, which become about 5.47dBm. In this study, only five ports were used and the others of three ports were terminated with 50Ω terminators.

2.5.4. Terminator

Figure2.9 shows the terminator. The impedance of this terminator is 50Ω and only five ports were used and connector shape is SMA-P. It can inhibit transmission and reflection of microwave at output port of divider.
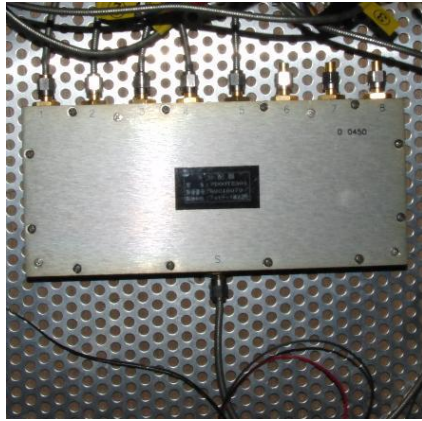
Figure2.8 Picture of 8-ways power divider (Left)

Figure2.9 Picture of 50Ω terminator (Right)

2.5.4. Digital phase shifter (6-bit)

Figure2.10 shows digital phase shifter "ArumoTech - FS01T2150". This phase shifter is digitally controlled by 6-bit signals from a computer. It is needed to input 12V-DC at No.9-pin of D-sub connector and to connect No.8-pin to ground. As a default position, 0V-DC has to be input into No.1 to No.6-pin and 5V are should be input into the pin which is wanted to operate. This phase shifting mechanism is represented in Figure2.11. The phase shifter digitally switches the electrical length of transmission line. As a result, this phase shifter can shift the microwave phases reradiate from horn antennas. Table2.2 shows amount of shifted phase of this phase shifter.

2.5.5. Driver amp

Figure2.12 shows the driver amplifier "RF Bay, Inc. - LPA-6-30". The input and output connector shape is SMA-J and operating voltage is 12V-DC. The gain of this amplifier is about 37dB. Maximum RF input power is 17dBm and P_{1dB} is 17dBm, IP3 is 32dBm. This driver amplifier amplifies the microwave power level after the phase shifters to compensate the power loss by the phase shifters.
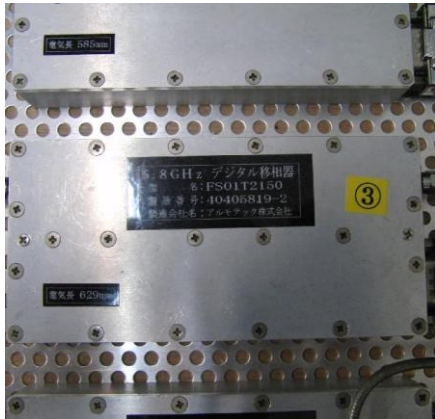
Figure2.10 Picture of digital phase shifter (Left)
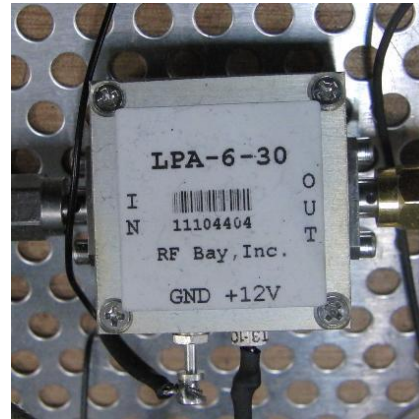
Figure2.12 Picture of driver amp (Right)
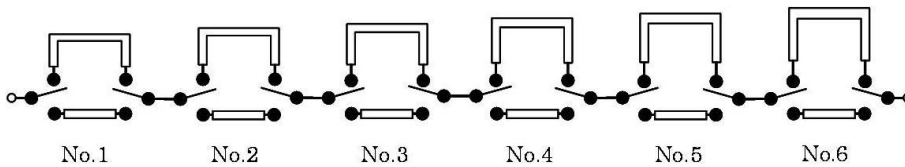
Figure2.11 Mechanism of phase shifter

Table2.2 Specification of phase shifter

D-sub pin No.	Function	Amount of shifted phase [deg.]
1	Bit No.1	5.625 ± 0.2
2	Bit No.2	11.25 ± 0.2
3	Bit No.3	22.50 ± 0.4
4	Bit No.4	45.00 ± 0.8
5	Bit No.5	90.00 ± 1.5
6	Bit No.6	180.0 ± 3.0
7		
8	GND	
9	DC+12V	

2.5.6. Power amp (1W)

Figure2.13 shows the power amplifier "RF Bay, Inc. - MPA-58-30". The input and output connector shape is SMA-J and operating voltage is DC+12V. The gain of this amplifier is about 30dB. Maximum RF input power is 20dBm and P_{1dB} is 30dBm, IP3 is 39dBm. This amplifier is FET

based type and boosts the microwave power to the desired level of about 1W. The sum of these five power amplifier outputs was about 5W, which we regarded as output power from transmitting system.

2.5.7. PCI board

The PCI board "Interface - PCI-2798C", the digital input and output module, is installed in the PC and it is controlled by LabVIEW. This PCI board can do analog-digital conversions at their 64 input-output ports. The voltage of input-output signal ranges from DC+5V toDC+48V and this PCI board does not need outside power supplies.

2.5.8. PCI connection board

Figure2.14 shows the PCI connection board "ArumoTech - SS00T2504". This PCI connection board connect PCI board and four phase shifters and transmit phase shifting signals.
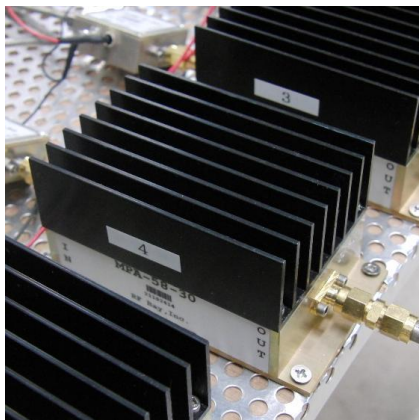
Figure2.13 Picture of power amplifier (Left)

Figure2.14 Picture of PCI connection board (Right)

These components are connected as shown Figure 2.15.
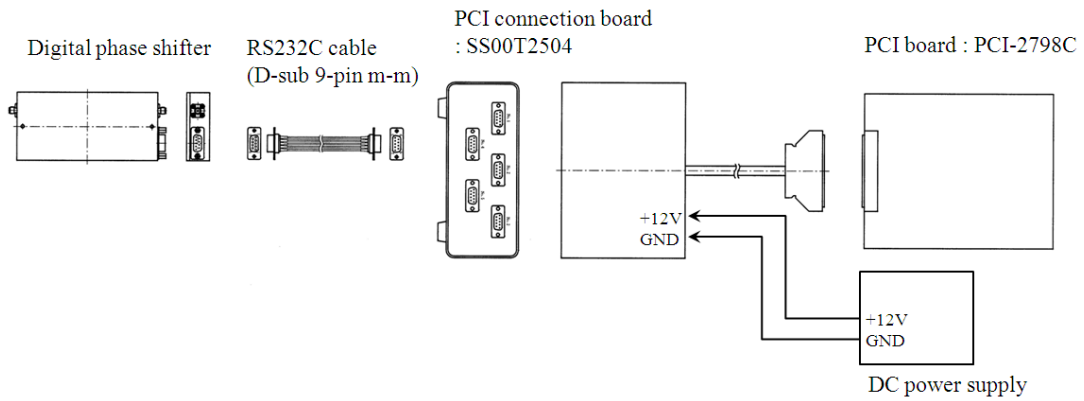
Figure2.15 Configuration diagram of digital components

2.5.9. Horn antenna

Figure2.16 shows the horn antenna and Figure2.17 represents the dimension of this horn antenna. The horn antenna is fine at its sharp directivity characteristics and high gain. So this antenna seems easy to be controlled and effective for a phased array element.
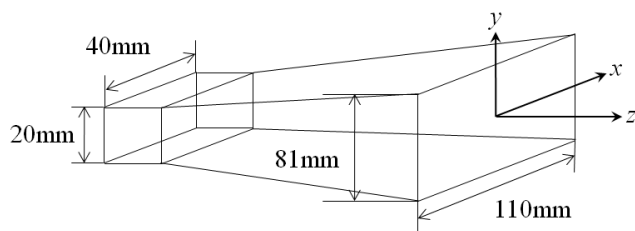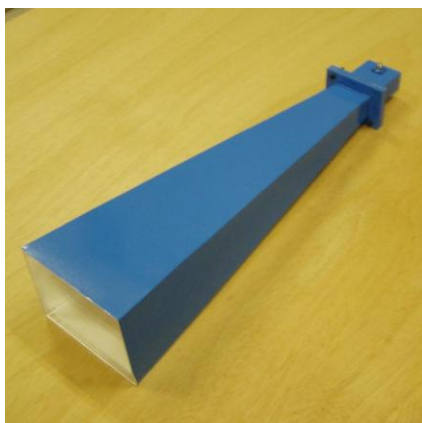
Figure2.16 Picture of horn antenna

Figure2.17 Dimensions of horn antenna

2.5.10. Metal grid circularizer

Circular-polarized wave is one of key factors to enable a stable power supply to MAVs. In this laboratory, horn antennas which support linearly-polarized waves are adopted, so linearly-polarized waves from horn antennas have to be transformed into circular-polarized waves. Therefore, a metal grid circularizer [7] is fabricated and integrated into transmitting system.

In this section, a basic theory and experimental results of the metal grid circularizer is introduced. A circular-polarized wave consists of two linearly-polarized waves whose phase difference is $\pi/2$. Thus, one linearly-polarized wave is equally divided into two linearly-polarized waves, same amplitude and same phase, and then a phase of one wave have to be added or subtracted $\pi/2$. Figure2.18 shows the structure diagram of the metal grid circularizer. The Mechanism of circularizer is that some metallic laminas whose width is w are arranged in equal distance s, and it is inclined at an angle of 45deg. with respect to direction of incident linearly-polarized wave. E_x wave which is x-axial component of E can pass the grid at propagation velocity of free space, but E_y wave passes the grid at phase velocity which depends on the gap between two metallic laminas (TE10 mode) as propagation in rectangular waveguides. Therefore, when w and s are chosen a proper length, a linearly-polarized wave can be transformed into a circular-polarized wave.

First, the phase velocities of E_x wave v_x and the phase velocities of E_y wave v_y are given by

$$v_x = c \quad , \quad v_y = c/\sqrt{1 - (\lambda_0/2s)^2} \tag{2.24}$$

Here c is velocity of light and λ_0 is free space wavelength. From Equation(2.24), the wavelength of E_y wave at the gap between two metallic laminas is expressed as

$$\lambda_s = \lambda_0/\sqrt{1 - (\lambda_0/2s)^2} \tag{2.25}$$

Then the phase condition, the phase difference between E_x wave and E_y wave have to be $\pi/2$, are following relation.

$$2\pi w/\lambda_0 - 2\pi w/\lambda_s = \pi/2 \tag{2.26}$$

Considering impedance matching, width of metallic laminas should be $\pi/2$ and each parameter is calculated as

$$w = 0.750\lambda_0 \quad , \quad s = 0.671\lambda_0 \tag{2.27}$$

In this study, because frequency of transmitting microwave is 5.8GHz, the width of metallic laminas is 38.8mm and the gap between two metallic laminas is 34.7mm.

Figure2.19 shows a picture of the metal grid circularizer. As will be find from this figure, gaps are filled with expanded polystyrene foams as reinforcement materials. Its dielectric constant is about 1.05 or less, so reinforcement materials can be ignored.

15
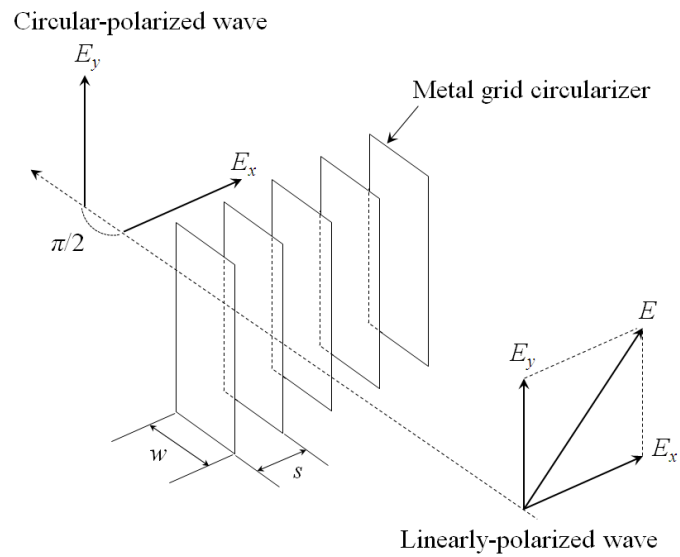
Figure2.18 Structure diagram of metal grid circularizer
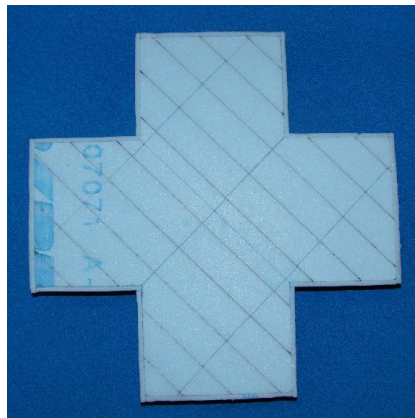
Figure2.19 Picture of metal grid circularizer

2.6. Experimental methodologies and results

2.6.1. Polarization of transmitting wave using the metal grid circularizer

Here the performance of the metal grid circularizer is represented in Figure2.20. The circularizer is set on a transmitting horn antenna array and a dipole antenna whose polarization is linear is set up at height of 500mm from the aperture plane of the horn antenna array. Then, yaw angle of the dipole antenna is rotated by each 15deg. between 0deg. to 360deg. and receiving powers at each yaw angle

are measured. In this case, the measurement dates are normalized by maximum value.

As will be find from this figure, electric fields E of the linearly-polarized waves from horn antennas are divided into two linearly-polarized waves, and they construct one electromagnetic wave whose polarization shape have x-axial component and y-axial component like a circular-polarized wave.
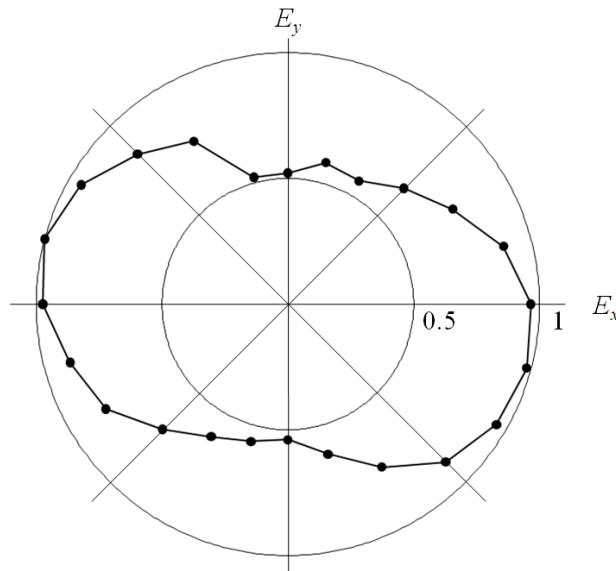
Figure2.20 Polarization of transmitting wave by using circularizer
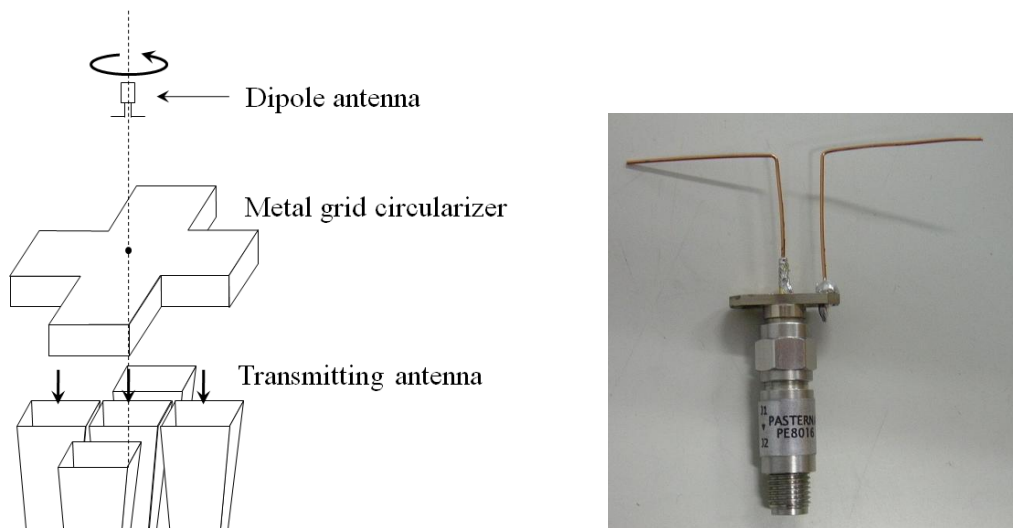
Figure2.21 Measurement setup of polarization

Figure2.22 Picture of dipole antenna

2.6.2. Beam profile of radiating wave from a phased array

In order to transmit a microwave beam to the target, the beam forming is a very important factor. At the transmitting system, five horn antennas are used as a phased array system, so phases of microwaves from each horn antennas have to be synchronized. Therefore, each phase shifters must be inputted the offset phases as default position to, because every component, for example, phase shifters, flexible coaxial cables, amplifiers, and horn antennas, have individual differences of electrical length. The measurement is done as following. The circular-polarized patch antenna (Figure2.22) which is connected to a power sensor "HEWLETT PACKARD – 8481A power sensor" (Figure2.23) is set up at height of 1500mm from the aperture plane of the horn antenna array. And then, to make receiving power peak which is printed on a power meter "HEWLETT PACKARD – 437B power meter" (Figure2.24), the phase shift signals, from +0deg. to +360deg., are inputted in four phase shifters. So, the offset phases which have to be inputted are measured by moment method. The result of measurement results are arranged in Table2.3.
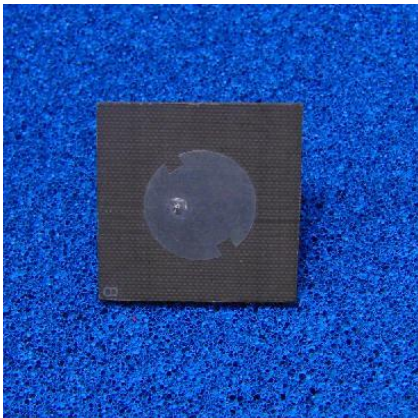
Figure2.22 Picture of 5.8GHz patch antenna

Figure2.23 Picture of power sensor

Figure2.24 Picture of power meter

Table2.3 Offset phases of each line

Line number	6-bit signal	Phase difference from No.1 [deg.]
No.2	47	262 - 267
No.3	30	166 - 172
No.4	14	76 - 81
No.5	50	279 - 284

Using the value of Table2.3 the beam profile is measured. Figure2.25 shows a measurement result of the radiation field from the horn antenna array and Figure2.26 shows a calculation result of it. As will be find from two figures, the measured and simulated result are good agreement with each other, and microwaves from five horn antennas form the ideal Gaussian beam like the calculate result. It proves two matters, one is that offset phases of each line are measured with accuracy, the other is that the metal grid circularizer does not affect the beam forming. Once the Gaussian beam is formed, the beam form does not change and the transmitting beam can keep its attenuation loss less between the transmitting antenna array and the MAV. But from the measurement result, the top of beam is a little lower than calculated result, because microwaves are attenuated by flexible coaxial cables and a little reflected at input ports of horn antennas before radiated.
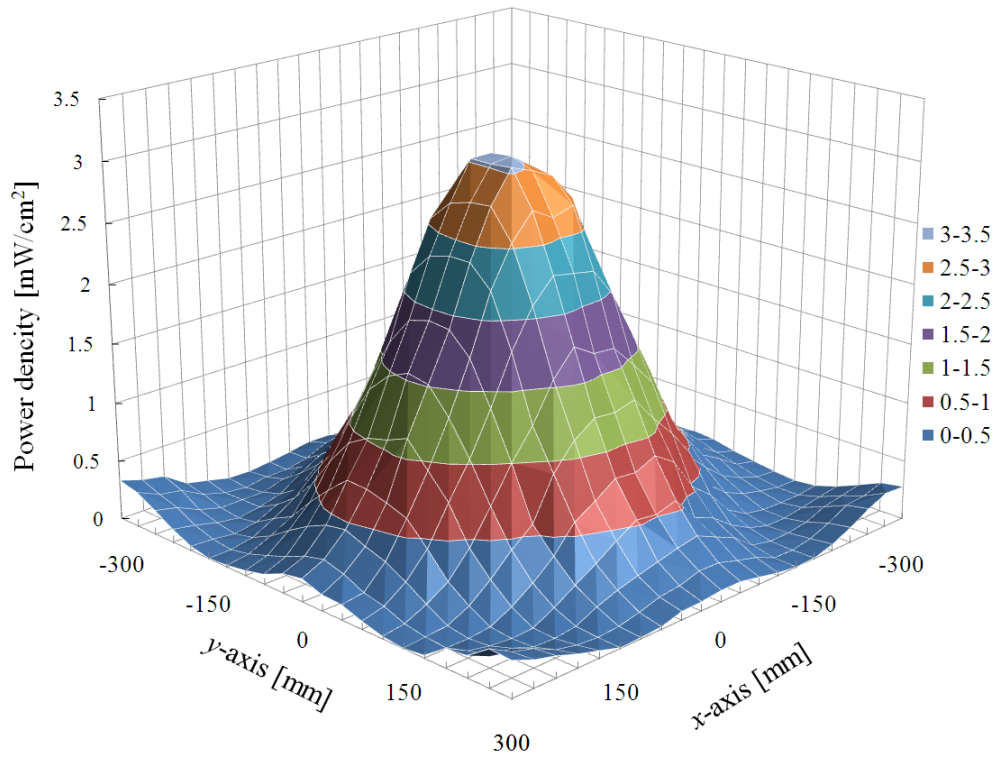
Figure2.25 Measured beam profile at *h*=1500mm
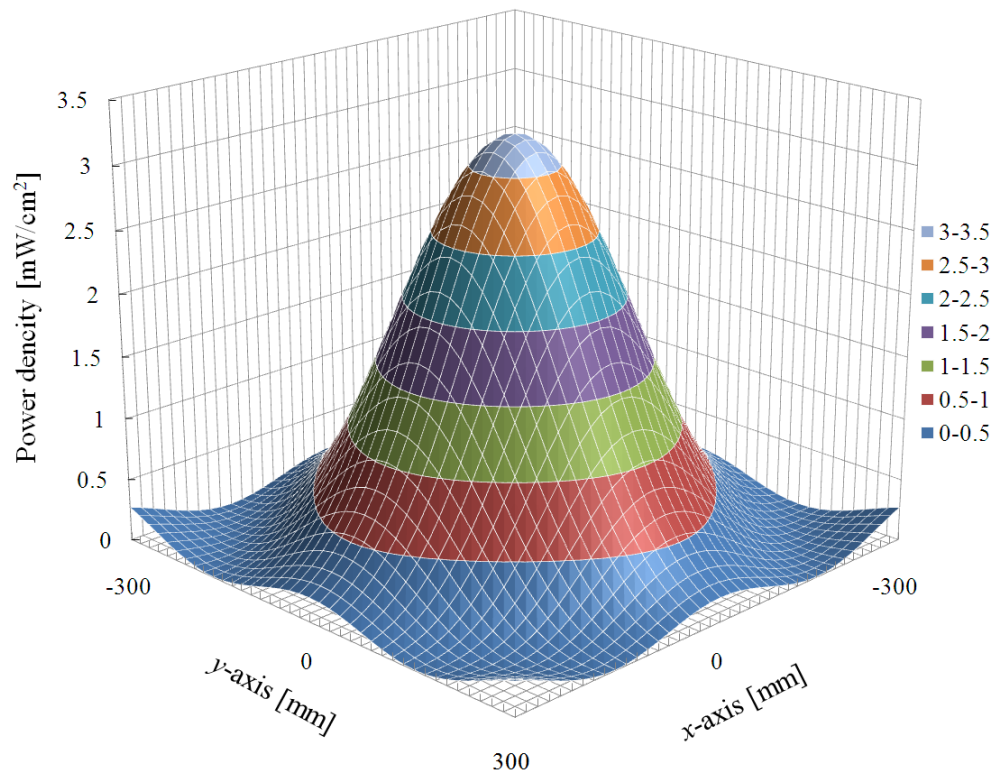
Figure2.26 Calculated beam profile at *h*=1500mm

20

2.6.3. Steering of the transmitting beam

In this section, the result of an Mr.Ozawa study is introduced. [8] In order to circle a microwave beam continually, radiation fields test with phase shifting signal which irradiated a certain points on the circle are done. The experiment condition is that the output power is 3.5W, a target circle with the radius of 160mm at 1040mm high is assumed. The experimental results are shown in Figure2.28, which are compared with the simulated data. The measured graphs represent with color the measured voltage distributions. And the simulated graphs represent the simulated power distributions. The power values were normalized by the maximum value in these four cases. In these graphs, the irradiating points are colored red to be easily recognized. And the irradiating point locations in the measured and simulated data are good agreement with each other. The whole distributions are also almost the same except gradients.

(a) Irradiation point is (160, 0, 1040)

(b) Irradiation point is (113, 113, 1040)

(c) Irradiation point is (80, 139, 1040)

(d) Irradiation point is (0, 160, 1040)
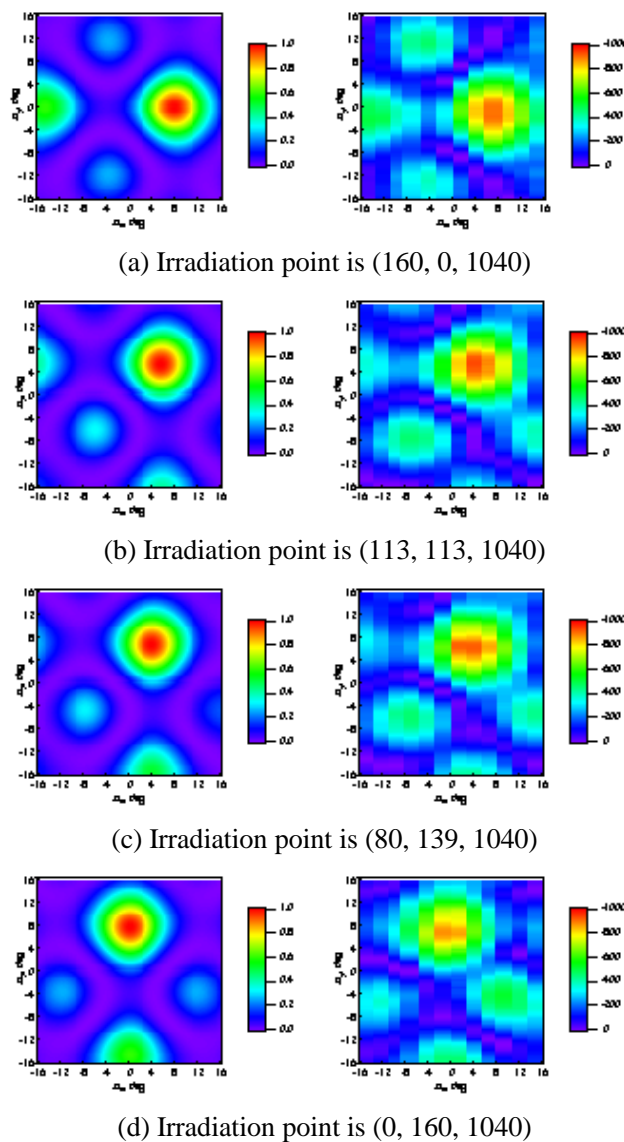
Figure2.27 Radiation field from 2D antenna array in measurement and calcuration

2.7. Summary of the transmitting system

At this section, the summary of the transmitting system is introduced. Figure2.28 shows the computed properties as a function of θ_{str}. The beam divergence was constant at about nine degrees, which corresponds to the beam quality of $M^2=1.6$. And Table2.4 shows the specifications of the transmitting system.
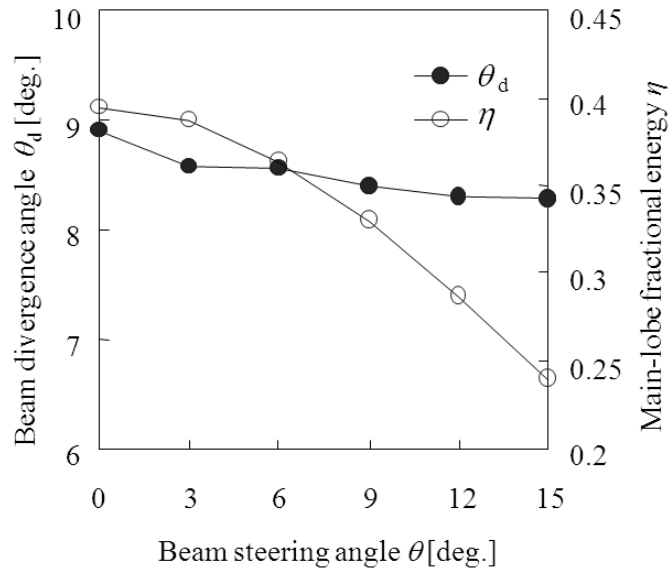
Figure2.28 Computed main-lobe fractional energy and beam divergence angle

Table2.4 Specifications of the five-element active phased array antenna

Parameters	Values
Microwave frequency	5.8GHz
Wavelength λ	51.7mm
Total transmission power P	5W
Array pitch d	110mm ($d/\lambda=2$)
Diameter of the array D	330mm
Beam quality M^2	1.6

Chapter 3.   Tracking system

3.1 System overview

In this section, a concept of the tracking system is introduced. To realize high efficiency wireless power transmission, detecting an MAV position is very important element because of pointing a microwave beam toward the MAV with accuracy. There are some detection methods, for example, image analysis, GPS, radar, hardware retro-directive. But in this study, software retro-directive function is adopted as the tracking system. "Phase of microwave" which is used at the phased array system is utilized to the tracking system. There are some advantage points of adopting it, for example, the theory is simple, the system can be compact, and the system readiness is fast, but the most challenging point is academic interest of how to use "Phase of microwave" which is the most interesting characteristic of wave phenomenon.

At the tracking system, the software retro-directive function is under development. This system receives a pilot signal of 2.45GHz microwave sent from the MAV and analyzes its current position using the phase difference.

3.2 Theory of tracking system

First, if there are two antennas with spacing d, the antennas receive the incident signals, which are expressed as

$$\boldsymbol{E}_0 = E_0 \exp j(\omega t) \tag{3.1}$$

$$\boldsymbol{E}_1 = E_1 \exp j(\omega t + \varphi_1) \tag{3.2}$$

Here φ_1 is the relative phase difference between these two antennas. When the free-space wavenumber is k, and the incident angle of a pilots signal is α, the phase difference becomes as

$$\varphi_1 = kd \sin \alpha \tag{3.3}$$

After this, the simple model which is expressed as Figure3.1 is assumed. If two antennas, one $+\varphi_0$ phase shifter, two dividers, one mixer, and three detectors are combined like this figure, the waves are expressed as

$$\boldsymbol{E}_0 = E_0 \exp j(\omega t + \varphi_0) \tag{3.4}$$

$$\boldsymbol{E}_1 = E_1 \exp j(\omega t + \varphi_1) \tag{3.5}$$

After phase shifting, the microwave is divided into two waves at each line, and then, by a power mixer, they are combined into the composite wave whose power depends on the amplitudes of two input waves. The composite wave is expressed as follow

$$\boldsymbol{P}_{\text{com}} = \left(\boldsymbol{P}_0{}^2 + \boldsymbol{P}_1{}^2\right)^2 \tag{3.4}$$

Applying the trigonometric functional equation to Equation(3.4)

$$P_{\text{com}} = P_0 + P_1 + 2\sqrt{P_0 P_1} \cos(\varphi_0 - \varphi_1) \tag{3.5}$$

Finally, detectors rectify power of the waves into voltage. The output voltage from the detector is liner proportional to input power, so the following equation is obtained.

$$V_{\text{com}} = V_0 + V_1 + 2\sqrt{V_0 V_1} \cos(\varphi_0 - \varphi_1) \tag{3.6}$$
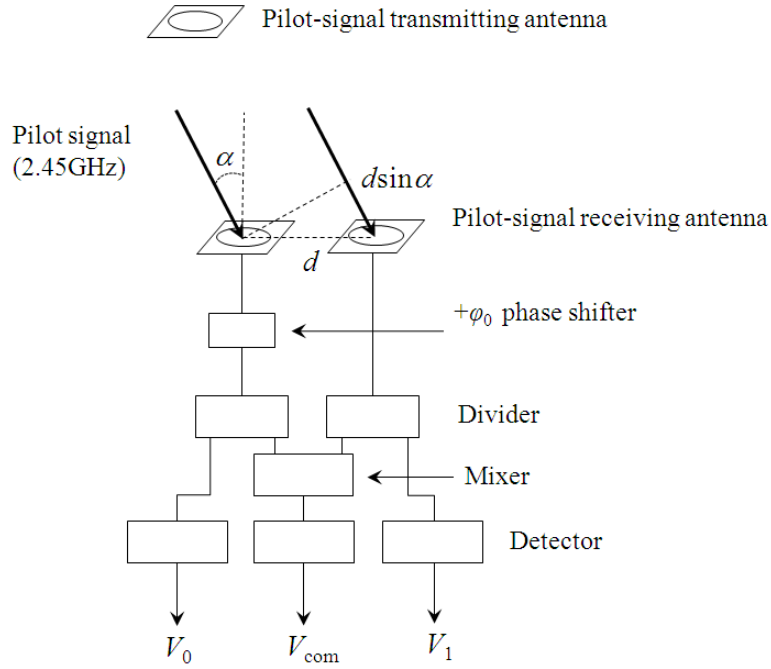
Figure3.1 Simple model of tracking system

If $+\varphi_0$ phase shifter is not combined, Equation(3.6) becomes as

$$V_{\text{com}} = V_0 + V_1 + 2\sqrt{V_0 V_1} \cos \varphi_1 \tag{3.7}$$

In both cases $\pm\varphi_1$, the composite wave voltages become the same value and are not differentiated, which is represented in Figure3.2.

$$V_{\text{com}}(\varphi_1) = V_{\text{com}}(-\varphi_1) \tag{3.8}$$

This is the reason for adding a certain phase shift to the line-0. In the previous study, φ_0 is decided as $\pi/2$, and Equation(3.6) is given by

$$V_{\text{com}} = V_0 + V_1 + 2\sqrt{V_0 V_1} \sin \varphi_1 \tag{3.9}$$

Figure3.3 represents this equation. As will be find from this figure, there is a one-to-one correspondence between the output signal V_{com} and the incident angle of a pilots signal α. Therefore, if the output signal is measured, the incident angle can be detected.

Actually, however, output signals V_0 and V_1 are affected by individual differences of each component, so they do not fulfill the Equation(3.9). Therefore, fitting coefficients η_0 and η_1 are

24

introduced. If fitting coefficients η_0 and η_1 are used, Equation(3.9) becomes as

$$V_{\text{com}} = \eta_0\big(V_0 + V_1 + 2\eta_1\sqrt{V_0 V_1}\sin\varphi_1\big) \tag{3.10}$$

If the pilot signal transmitting antenna is far from two pilot signal receiving antennas, the receiving signal E_0 and E_1 are almost the same level of intensity. So, the value of V_0 is largely similar to V_1, and Equation(3.10) is given by

$$V_{\text{com}} = 2\eta_0 V_1(1 + 2\eta_1\sin\varphi_1) \tag{3.11}$$
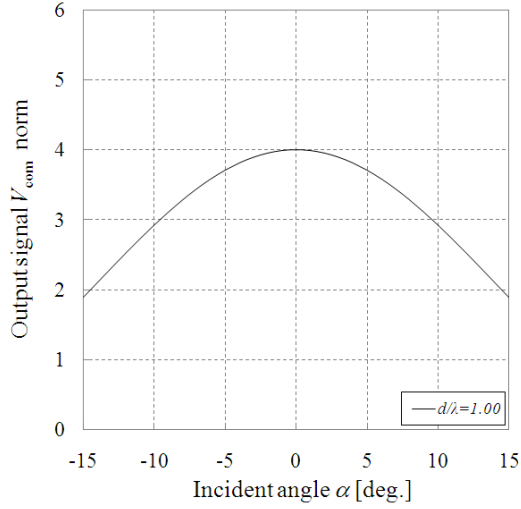
Figure3.2 V_{com} without any insertion phase to line-0 (Left)
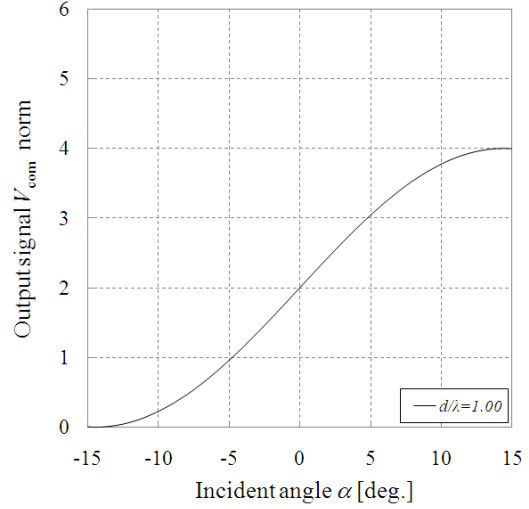
Figure3.3 V_{com} with $+\pi/2$ phase shifting at line-0 (Right)

3.3. Experimental setup of tracking system

Basing the simple model of tracking system, the two type 2D tracking systems are suggested and these diagrams are shown in Figure3.4 and Figure3.5. Type1 uses only three pilot signal receiving antennas but Type2 uses four. At the Type1 tracking system, the dividers and mixers are complexly connected but the devices of x-direction and y-direction are independent at Type2. Firstly 2.45GHz microwave are radiated from a flexible circular-polarized patch antenna with an oscillator. Then three of four circular-polarized patch antennas which are arrayed two dimensional receive the pilot signal. As will be find from Figure3.4 and Figure3.5, the pilot-signal receiving antennas are arranged crosswise on the x-axis and y-axis. And spacing d_1 was set to 170mm which is about 1.39λ. And next, the microwaves pass into the quarter-wave line and they are added $+\pi/2$ phase difference comparing with unpassed microwaves on each axis. The amplifiers amplify microwaves power up to necessity level and microwaves are become output signals V_1 and V_{com1}, V_2 and V_{com2}, thorough the power dividers, the mixers, and the detectors.

25

2.45GHz oscillator

2.45GHz flexible circular-polarized patch antenna

Circular-polarized patch antenna

Quarter-wave line

Amplifier

Power divider

Mixer

Detector

V_2 V_{com2} V_{com1} V_1

PC

BNC connector box

Horn antenna

d_1

d_1

Pilot-signal receiving antenna
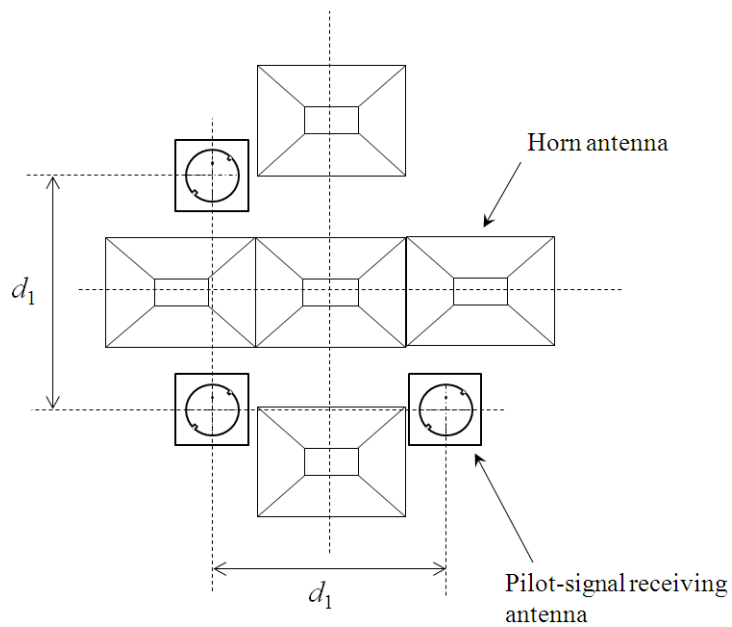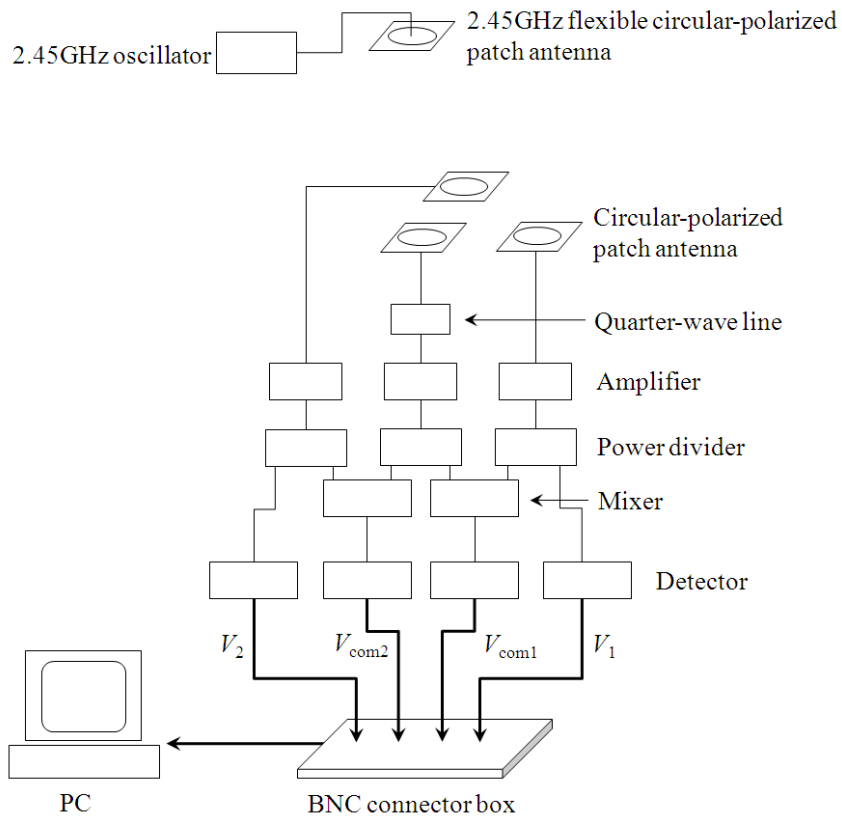
Figure3.4 Diagram of 2D tracking system (Type1)

26

2.45GHz oscillator

2.45GHz flexible circular-polarized patch antenna

Circular-polarized patch antenna

Quarter-wave line

Amplifier

Power divider

Mixer

Terminator

Detector

V_2 V_{com2} V_{com1} V_1

PC

BNC connector box

Horn antenna

d_1

d_1

Pilot-signal receiving antenna
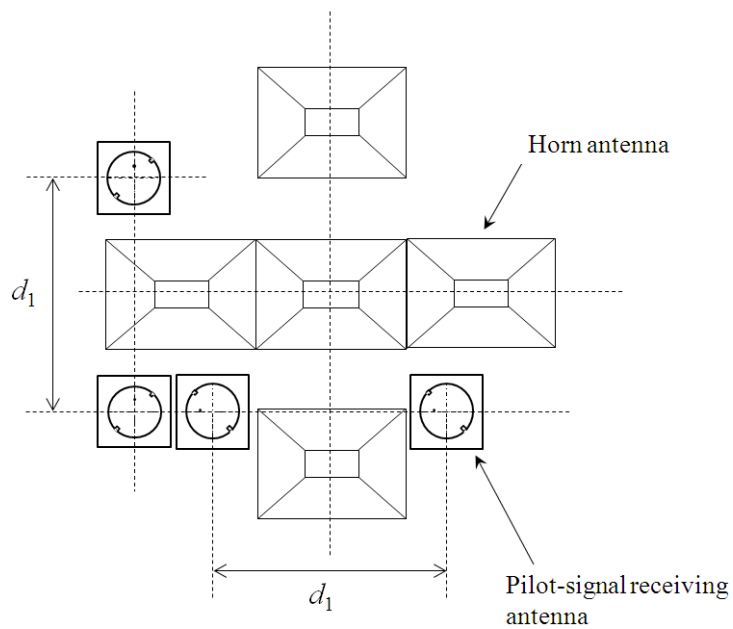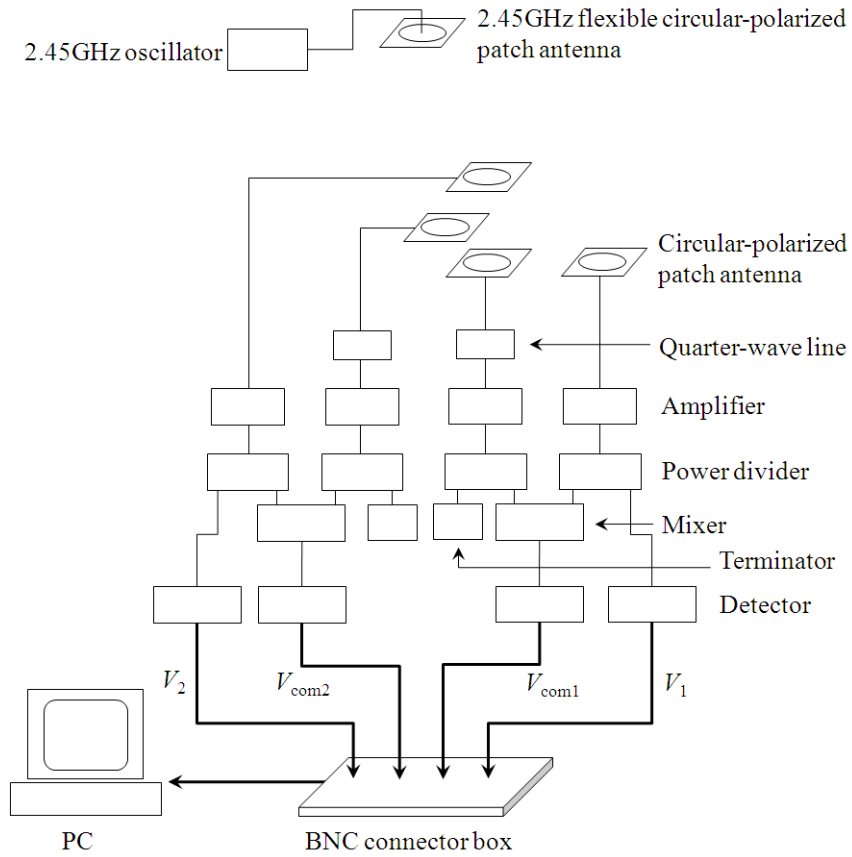
Figure3.5 Diagram of 2D tracking system (Type2)

3.4. Experimental devices of tracking system

3.4.1. 2.45GHz oscillator

Figure3.6 shows the 2.45GHz oscillator "ArumoTech - OS00T2436". This oscillator is composed of plate-tuning method and Metal Oxide Semiconductor Field Effect Transistor. The Output connector shape is SMA-J and operating voltage is DC+12V. The output power is stable and about 10dBm.
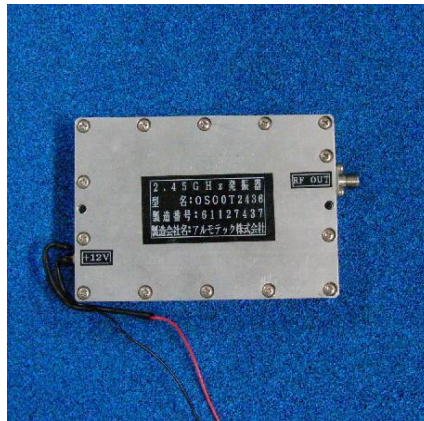
Figure3.6 Picture of 2.45GHz oscillator (Left)

3.4.2. 2.45GHz flexible circular-polarized patch antenna

Figure3.7 shows the 2.45GHz flexible circular-polarization patch antenna. This antenna is developed in our laboratory as the pilot-signal transmitting antenna. To make antenna flexible, the felt pad whose dielectric constant ε is 1.003 is adopted as the dielectric basal plate of circular-polarized antenna because it will be attached on curved surface of the MAV wing. And SMA-J connector is used for the feeding point. The dimension of the antenna is shown in Figure3.8.
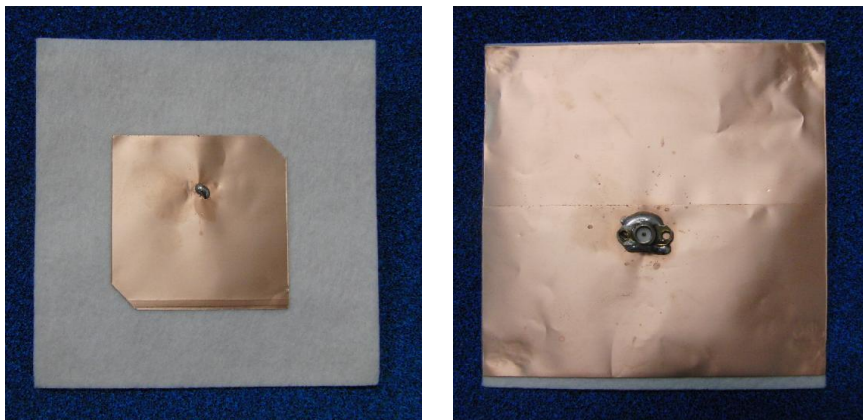
Figure3.7 Picture of pilot-signal transmitting antenna

28
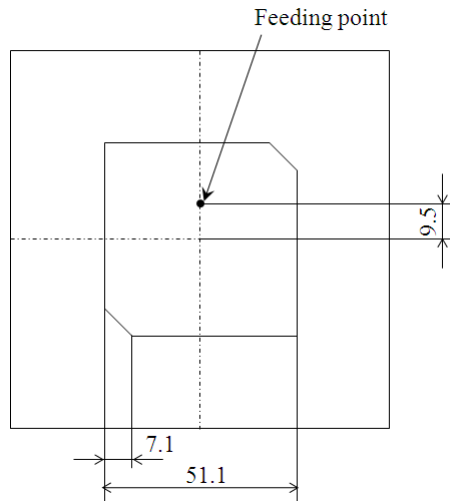
Figure3.8 Dimension of 2.45GHz flexible circular-polarization patch antenna (Right)

3.4.3. 2.45GHz circular-polarization patch antenna

The 2.45GHz circular-polarization patch antenna is used as the pilot-signal receiving antenna. This antenna is manufactured by JRC Nihon Musen Co., Ltd. Hard dielectric material is used at its basal plate, but there is no problem to use in the tracking system on the ground. The size of four antennas is shown in Figure3.9. Dimension of antennas are difference because their dielectric basal plates are cut at previous study.

3.4.4. Quarter-wave line

Figure3.10 shows the quarter-wave line which is manufactured by ArumoTech. The electrical length of this line is one-fourth of wave length at 2.45GHz, and input and output connector shapes are SMA-P. If a microwave are transmitted through the quarter-wave line, the phase of output microwave are delayed its phase $\pi/2$ comparing with input wave.

3.4.5. Amplifier

Figure3.11 shows the amplifier "Mini-Circuits –ZX60-2534+". The input and output connector shape is SMA-J and operating voltage is from DC+2.8V to DC+5V, and frequency range is from 0.5GHz to 2.5GHz. The gain of this amplifier is 35dB or more at 2.45GHz DC+5V. The maximum ranges of each parameter are: DC voltage 7V, Input power -15dBm, Output power 1W. Without this amplifier, the incident angle of pilot signal is difficult to be detected because output signal range between peak (the phase difference is 0deg.) and least (the phase difference is 180deg.) become narrow.

29
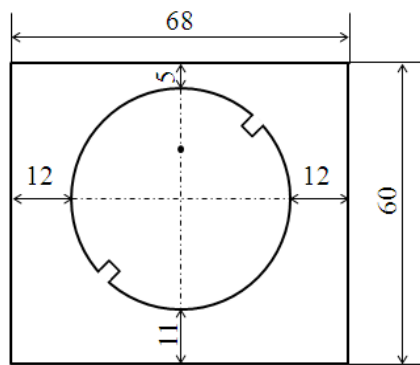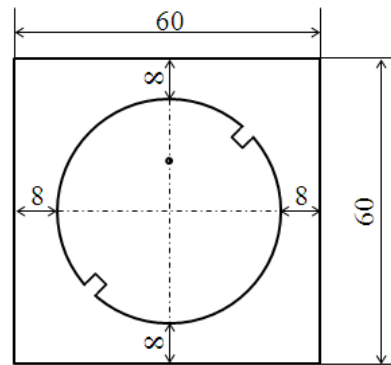
antenna 1

antenna 2
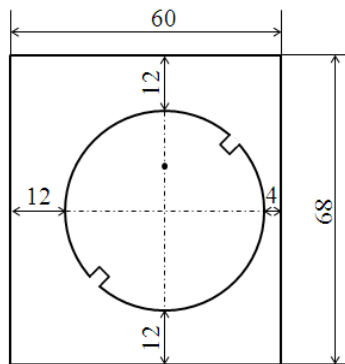
antenna 3
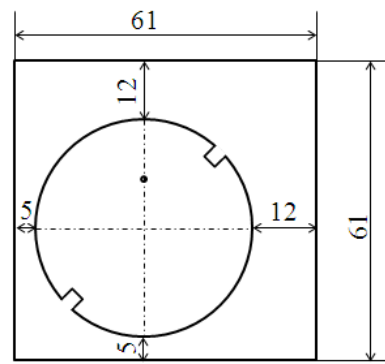
antenna 4

Figure3.9 Dimension of four pilot signal receiving antenna

Figure3.10 Picture of quarter-wave line (Left)

Figure3.11 Picture of amplifire (Right)

3.4.6. Power divider

Figure3.12 shows the power divider "ArumoTech - PD00T2519". At this power divider, the microwave from each amplifier is divided into two. The frequency range of this divider is from 1.7GHz to 9GHz and the insertion loss is less than 1.4dB. Maximum input power in +20dBm and the input and output connector shape is SMA-J.

3.4.7. Mixer

Figure3.13 shows the mixer "ArumoTech - PD00T2437". At this mixer, the microwave from each divider is mixed into one. The frequency range of this mixer is from 2.4GHz to 2.48GHz.

Figure3.12 Picture of power divider

Figure3.13 Picture of mixer

3.4.8. Terminator

Figure3.14 shows the terminator. The impedance of this terminator is 50Ω and only five ports were used and connector shape is SMA-P. It can inhibit transmission and reflection of microwave at output port of divider.

3.4.9. Detector

Figure3.15 shows the detector "Pasternack Enterprises, Inc. - PE8016". In this detector, the schottky diode is used for rectifying the microwave. The input connector shape is SMA-P and the output connector shape is SMA-J. The frequency range is from 2.0GHz to 8.0GHz, and the maximum input power is +23dBm. The minimum voltage sensitivity is 500mV/mW.

Figure3.14 Picture of terminator

Figure3.15 Picture of detector

3.4.10. BNC connector box

Figure3.16 shows the BNC connector box "Interface - TMR-7101". Using this connector box, the amphenol connector is converted into BNC connector and it can be easy to send the signal between the amphenol connector and the BNC connector. It has 50 pins of input and output ports, so some signals can be used at the same time. In this study, the input signal is the single-end type, so the receptacles have to be installed at jumper switches inside of this connector box.
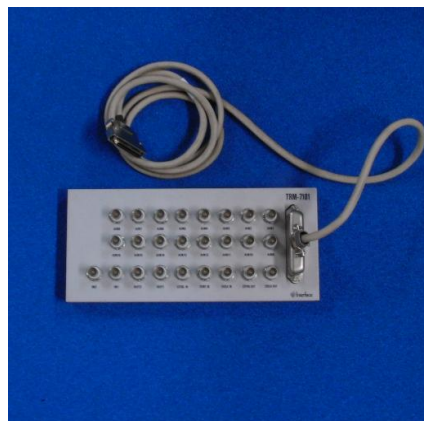
Figure3.16 Picture of BNC connector box

3.4.11. PCI board

The PCI board "Interface – PCI-3120", the analog input and digital output module, is installed in the PC and it is controlled by LabVIEW. This PCI board can do 12-bit analog-digital conversions and 8 channels sampling at the same time. The conversion time is $16\mu s$. The voltage range of input signal is from 0V toDC+10V at unipolar , from DC±5V to DC±10V at bipolar.

3.5. Experimental methodologies and results

3.5.1. Measurement of relationship between the incident angles and the output voltage

First, in order to detect the target position, the relationship between the incident angles of pilot signal α and the output voltage V_1 and V_{com1} have to be evinced. From the Equation(3.3) and (3.11), these equations become

$$V_{com}/V_1 = 2\eta_0(1 + 2\eta_1 \sin(kd \sin \alpha)) \qquad (3.12)$$

So, fitting coefficients η_0 and η_1 have to be decided from measurement result. To get the value of η_0 and η_1, the pilot signal transmitting antenna with the 2.45GHz oscillator is set at height of 500mm from the pilot signal receiving antennas, and it was slid as the incident angle α become each degree from -15deg. to +15deg. And output signals are measured by using the oscilloscope "Tektronix - TDS2004B" (Figure3.17). The measurement set up is represented in Figure3.18. In this measurement, Type1 tracking system is adopted. The distance of two pilot signal receiving antennas are 170mm, so the target whose incident angle is between -10.4deg. to +10.4deg. can be detected.

The result is shown in Figure3.19. As will be find from this figure, the curve is very smooth and one-to-one correspondence between V_{com1}/ V_1 and α can be found. But the range between peak and least of output signal is very narrow comparing with the theory. Because at the Type1 tracking system, the dividers and mixers are complexly connected, so the microwaves which are transmitted in these devices counterflow toward other components and construct the standing wave.

Figure3.17 Picture of oscilloscope
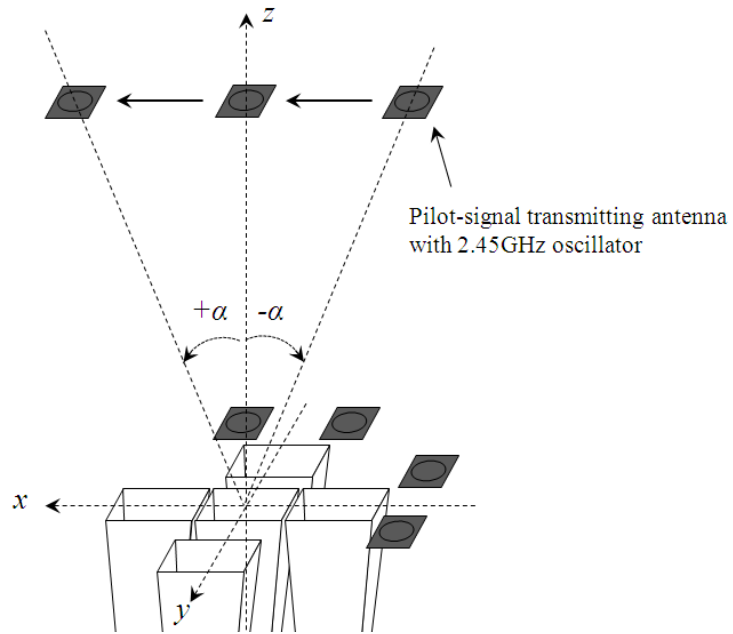
Figure3.18 Measurement setup of this experiment
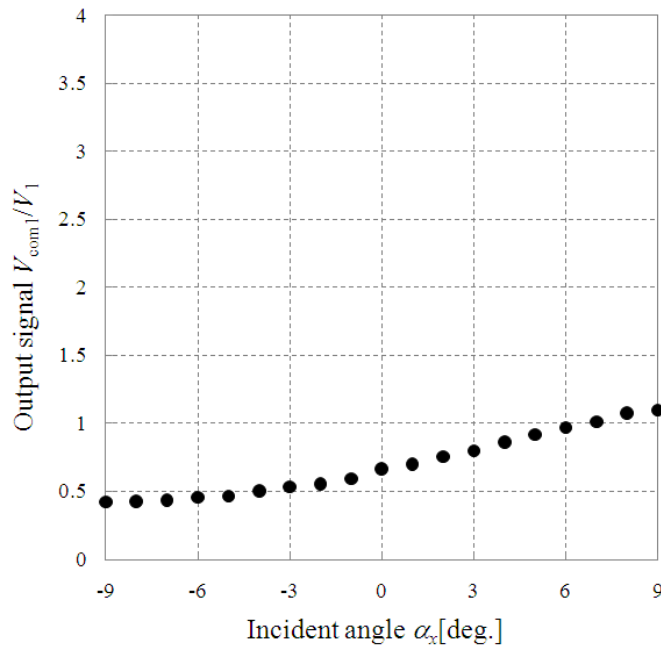
Figure3.19 Result of Type1 tracking system (*x*-direction)

Therefore, Type2 tracking system is adopted. The measurement set up is almost same, but the pilot-signal transmitting antenna is set at height of 1000mm. The result of *x*-direction is shown in Figure3.20, *y*-direction is shown in Figure3.21. At these figures, the corrections are considered. As

will be find from this figure, the curve is very smooth and one-to-one correspondence can be found. And the range between peak and least of output signal become wider than the result of Type1. From these results, the fitting coefficients η_0 and η_1, η_2 and η_3 are decided as

x-direction: $\eta_0 = 1.12$, $\eta_1 = 0.56$

y-direction: $\eta_2 = 1.22$, $\eta_3 = 0.41$
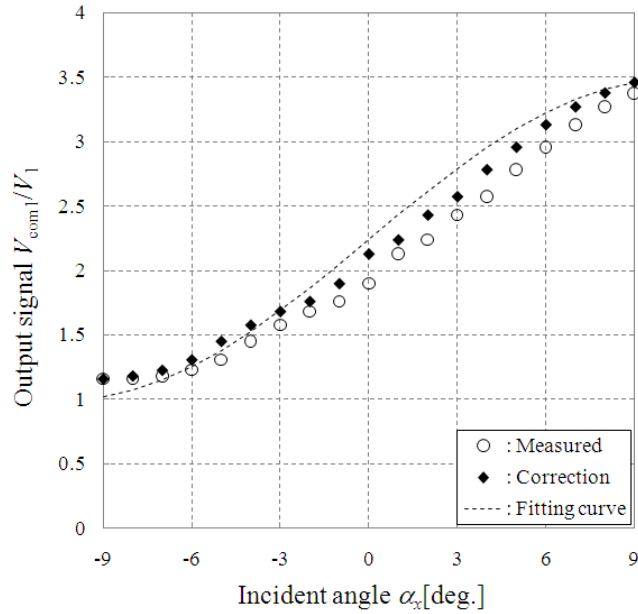
Figure3.20 Result of Type1 tracking system (x-direction)
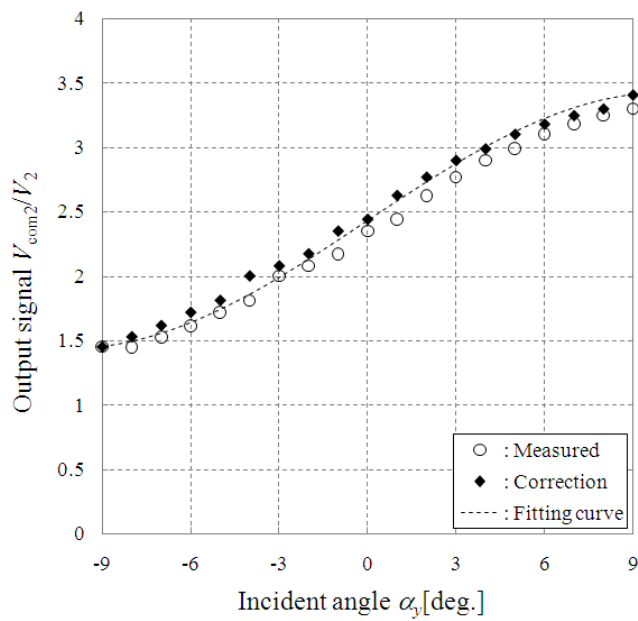
Figure3.21 Result of Type1 tracking system (y-direction)

3.5.2. 2D tracking demonstration test using circling MAV model

Next, the demonstration test of 2D tracking is done. To simulate the MAV circling, the pilot-signal transmitting antenna with the 2.45GHz oscillator is attached at the rotation equipment which is constructed from a supporting bar and a electrical motor. And they are set at the altitude of 1000mm and the rotation radius was 100mm which are corresponding incident angle was 5.7 degree. The rotation period was 0.79 second per round. That is, the rotation speed was 75.9 rpm.

Figure3.22 shows the estimated incident angles using the correlation shown in Figure3.20 and Figure3.21, and the estimated positions are plotted in Figure3.23. As will be find from this figure, the each waveform of α_x and α_y are similar to ideal sine wave which is the theoretical shape. The width between a peak and next peak is found at 0.79 second and the peaks of each waveform become about 5.7 degree. From this result, this 2D tracking system can, approximately, detect the MAV circling.

But the each waveform of α_x and α_y has some deformation points. The factor of these deformations is the reflections of microwave. The pilot signal is reflected at surrounding objects, for example a ceiling panel, a floor panel, devices of the tracking system, and horn antennas which is set near the pilot signal receiving antennas, and the antennas catch reflected waves as a noise. And there is a problem at the antenna in itself. As will be find from Figure3.9, the dimensions of dielectric basal plates have individual differences and the narrowest width of them is only 4mm. So, electrical fields are radiated from the edges of antennas and such fields are caught by other antennas as a noise. And then, the polarization shapes of each antenna may be the factor of deformations. Figure3.24 shows the polarization shapes of antenna1 and antenna2. As will be find from this figure, the polarization shapes of each antenna have individual differences, and the polarization shapes of pilot signal transmitting antenna is not pure circle. Therefore, receiving powers of each antenna are always changing while the MAV circling because the MAV changes its yaw angle. The tracking system detects the MAV position from receiving powers of each antenna, so this matter may be one of the problems.

Therefore, if these problems are solved, the waveforms become pure sine curves.

36
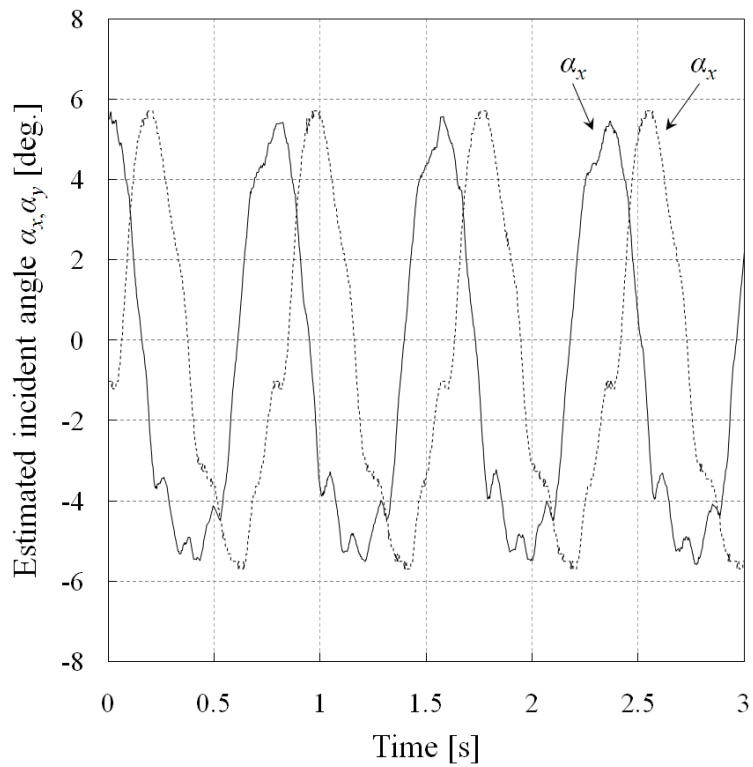
Figure3.22 Estimated incident angles α_x and α_y while the MAV model is circling
at the radius of 100mm and the altitude of 1000mm
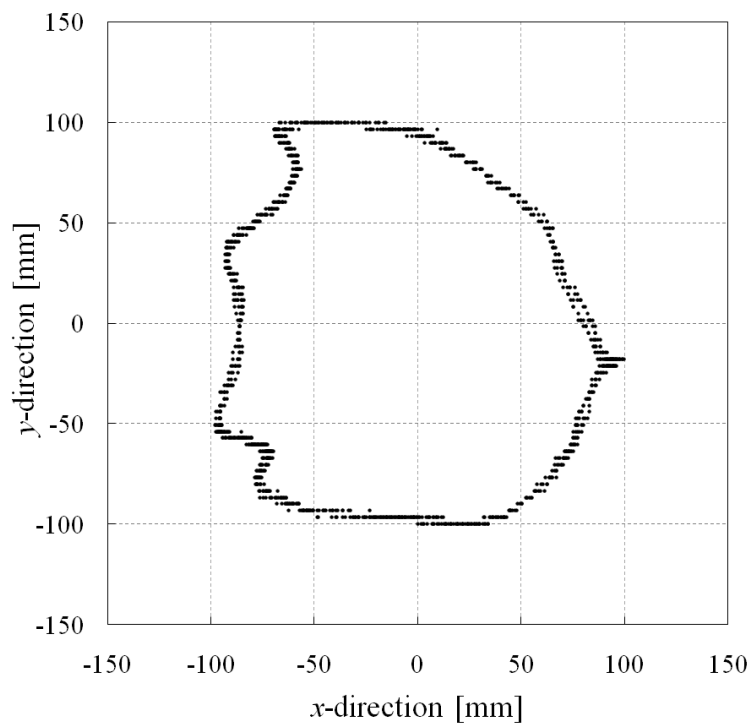
Figure3.23 Estimated position of the MAV model
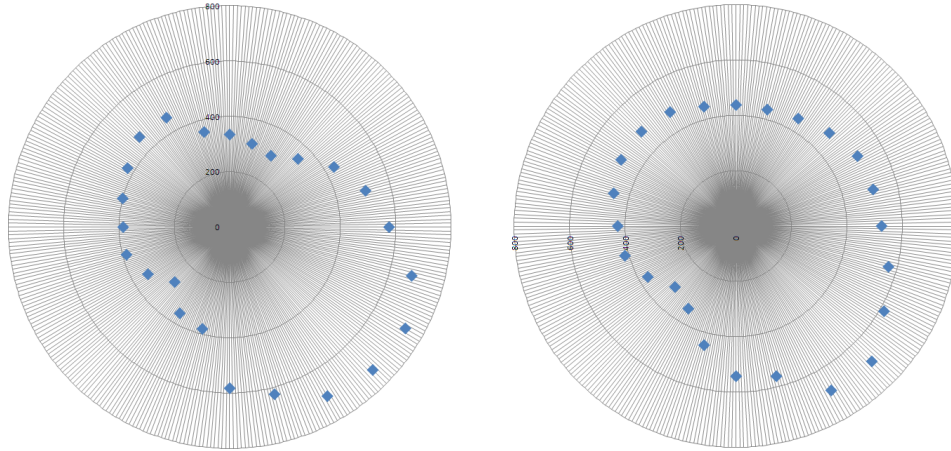
Figure3.24 Polarization shapes of antenna1 (Left) and antenna2 (Right)

3.5.3. Accuracy evaluation of 2D tracking

Accuracy evaluation is a something that must be done at the tracking system. In this section, the error between the estimated position and actual position of the MAV model are calculated. First, at the beginning with evaluating the accuracy of tracking performance, the coordinates are changed from x-axis and y-axis to radial-direction and azimuth-direction as shown in Figure3.25 and Figure3.26. A direction of movement is defined as the azimuth-direction, and a direction normal to movement is defined as radial-direction. From the estimated incident angles α_x and α_y, the errors of such directions are calculated and described in the solid angles. Figure3.27 shows the error of α_{rad}, Figure3.28 shows the error of α_{azi}.

As will be find from Figure3.27, the error of α_{rad}, is oscillating between about -1.5deg. to about 1.5deg. The maximum error is -1.65deg. (absolute value is 1.65deg.) at measurement time is 1.65seconds. Given that the 5.8GHz transmitting beam divergence is 9deg., the error 1.65deg. is sufficiently small. And then, from Figure3.28, the error of α_{azi} is oscillating between about -3deg. to about 3deg. The maximum error is -3.06deg. (absolute value is 3.06deg.) at measurement time is 0.05seconds. This value is sufficiently small, too.

However, α_{azi} have a large margin of error comparing with α_{rad}. It is because the motor which is used in the rotation equipment is not stable well. The oscillator and batteries are a little heavy, so if the light weight oscillator is used and the MAV can transmit the pilot signal by receiving power, the error value of α_{azi} can become lower.
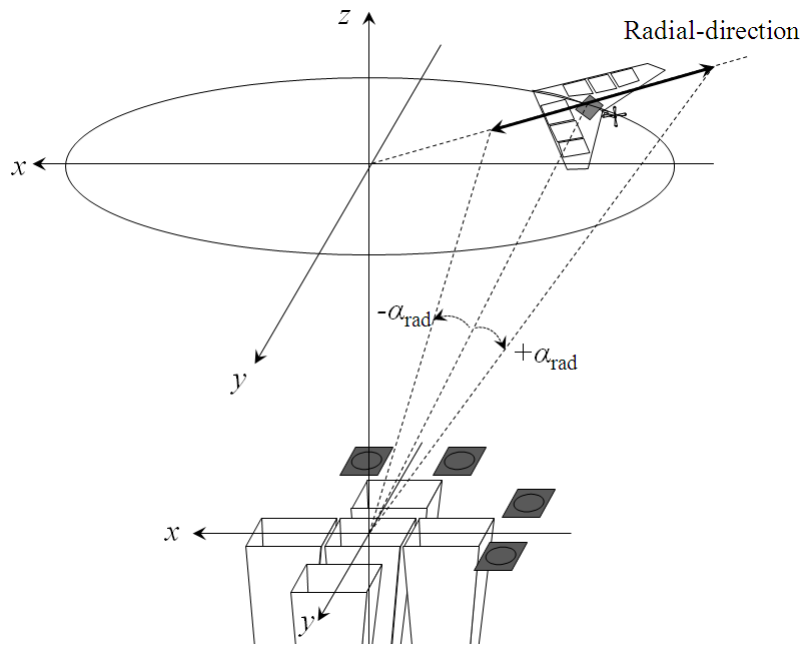
Figure3.25 Description of radial-direction
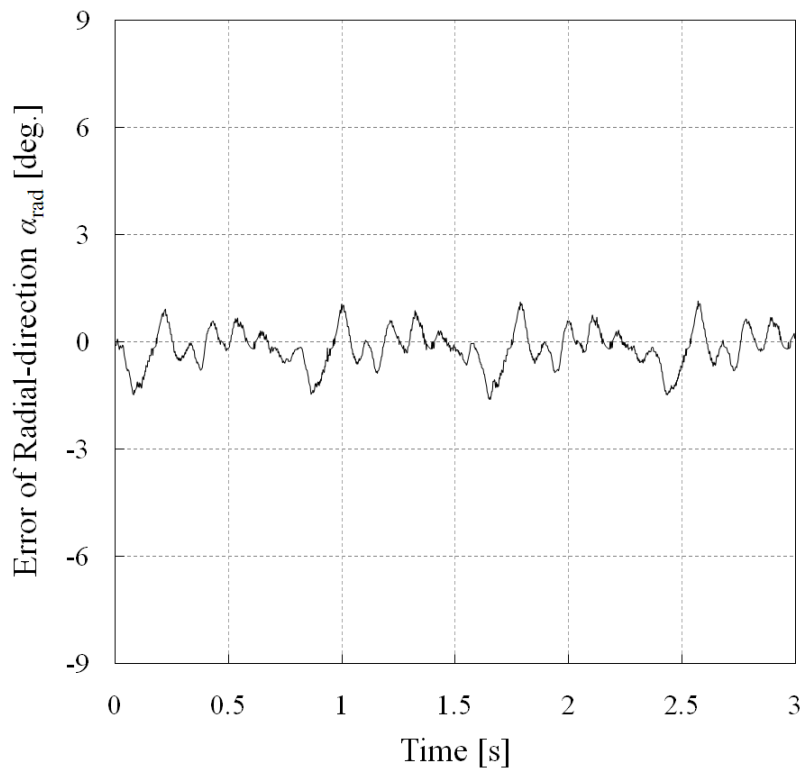
Figure3.27 Error of Radial-direction α_{rad}
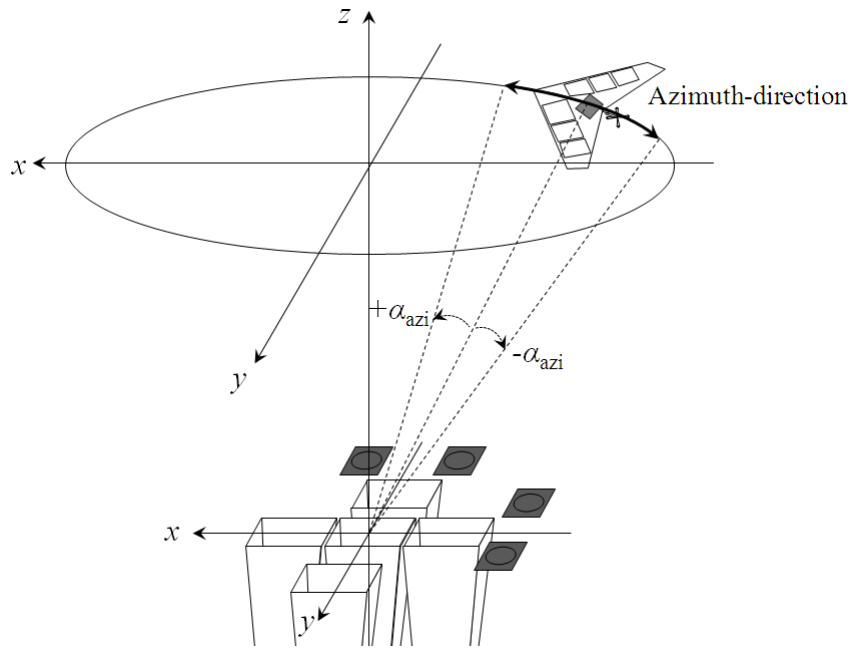
Figure3.26 Description of azimuth-direction
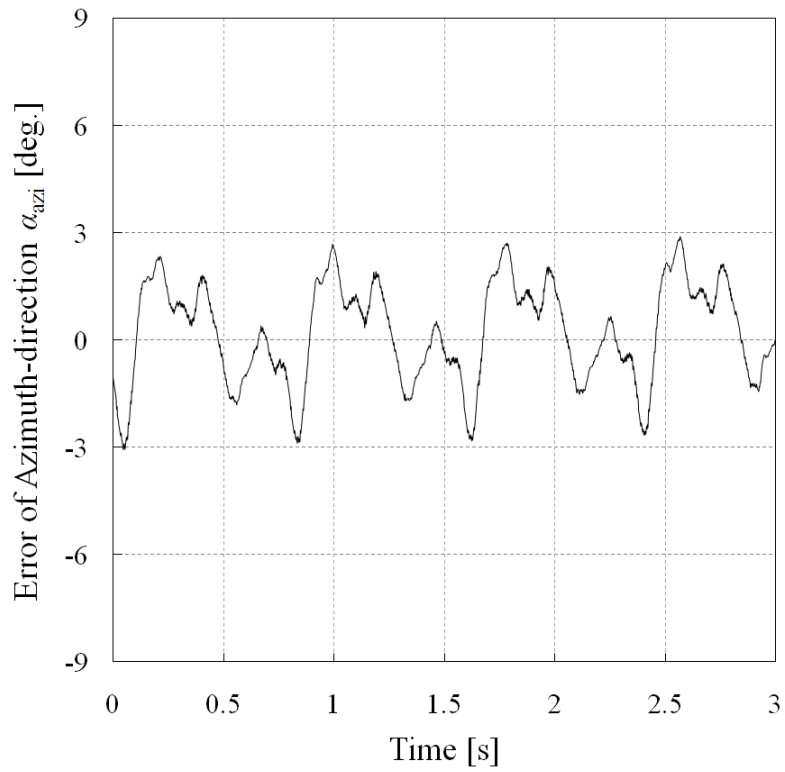
Figure3.28 Error of azimuth-direction α_{azi}

Chapter 4. Receiving system

4.1 Performance of rectenna

In this section, the performance of rectenna is introduced. As a receiving system, the light-weight flexible patch rectenna is developed in our laboratory as shown in Figure4.1. To make the rectenna flexible, the felt pad whose dielectric constant ε is 1.003 whose thickness is 1mm is adopted as the dielectric basal plate. And the cupper tape whose thickness is 0.1mm is used at antenna and transmission lines. The schottky barrier diode "NEC - 1ss97" is used at the rectifier circuit.
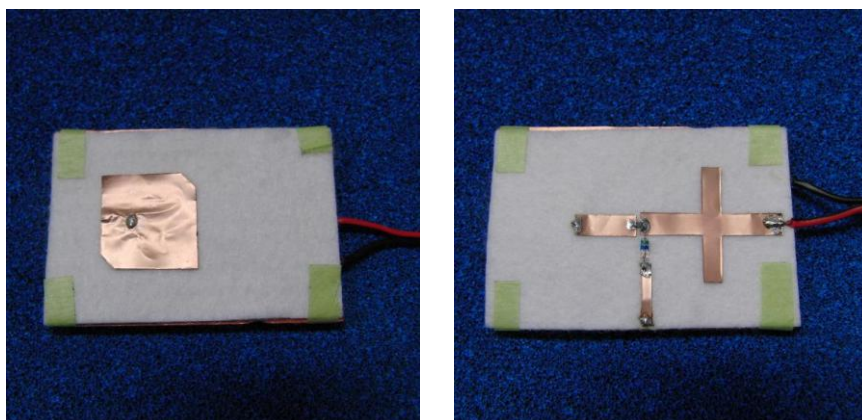
Figure4.1 Picture of rectenna (antenna side (Left), rectifier circuit side (Right))

Figure4.2 shows the relationship between the road resistance and RF-DC conversion efficiency of the rectifier circuit. As will be found from this figure, the maximum conversion efficiency is about 20.5% at the 100Ω. It means that the road resistance which is matched to the rectifier circuit is 100Ω.

Figure4.3 shows the relationship between input power and rectenna efficiency at 100Ω road resistance. As will be found from this figure, the rectenna efficiency is growing up until the input power is about 63mW, but after that the rectenna efficiency is decaying.
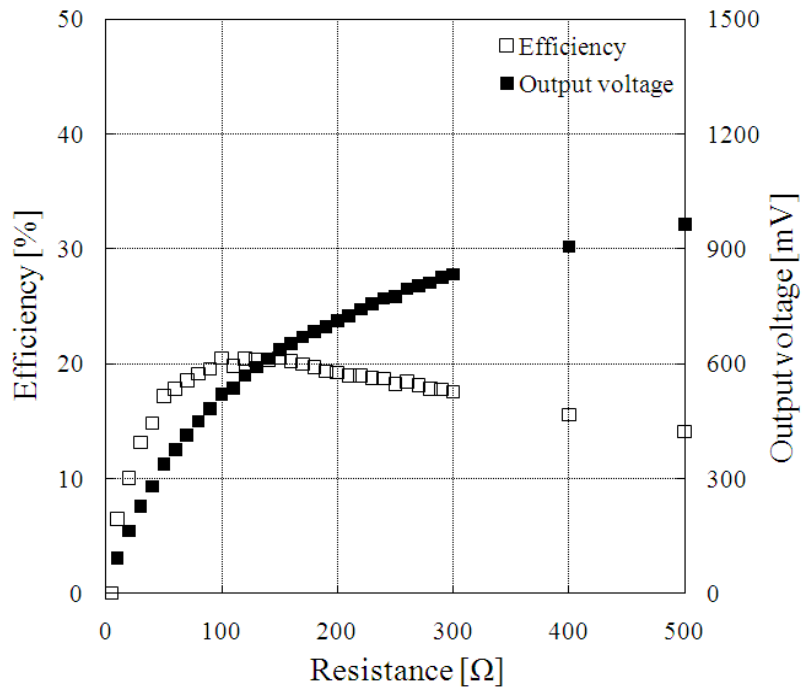
Figure4.2 Impedance matching of rectifier circuit
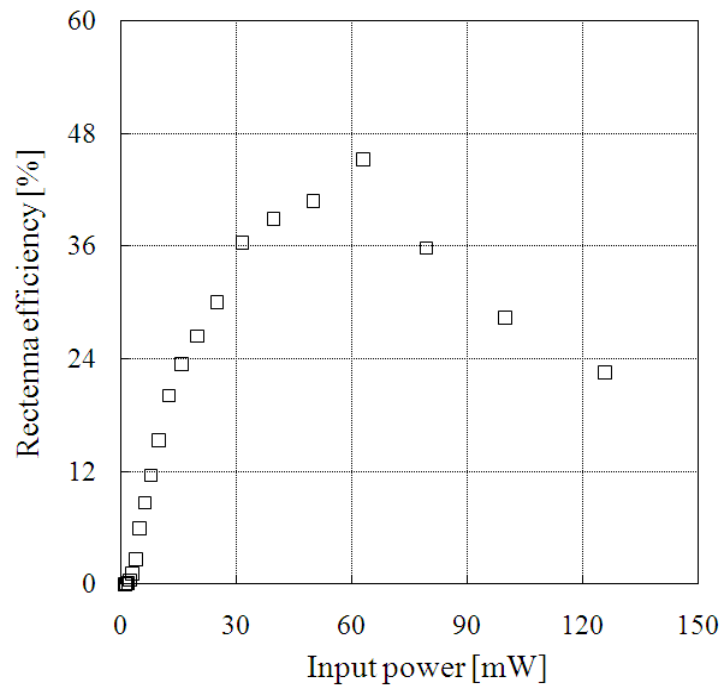

Figure4.3 Rectenna efficiency at 100Ω road resistance

Chapter 5. System integration and Demonstration

5.1 Integration of ground systems (transmission system and tracking system)

In this section, the process of the system integration is introduced. First, to integrate the transmitting system and the tracking system, these antennas arrangement have to be reconsidered because the metal grid circularizer of transmitting system has about 50mm thickness. If positions of the pilot signal receiving antenna are not moved, the circularizer would intercept the pilot signal which has to be caught by antennas of tracking system. So, the pilot signal receiving antennas are set up at height of 50mm from the aperture plane of the transmitting antenna array as shown in Figure5.1. However, by this change, the pilot signal receiving antennas have come to catch the noise which is reflected at horn antennas. Therefore, the antennas are surrounded by radio wave absorbers "Tohoku Chemical Industries, LTD - UFS-20" and then they are wrapped by metallic foils as shown in Figure5.2. The absorbers can attenuate only -20dB at 3GHz, so it does not absorb the reflection wave completely.


Figure5.1 Arrangement of tracking antennas and transmitting antenna array
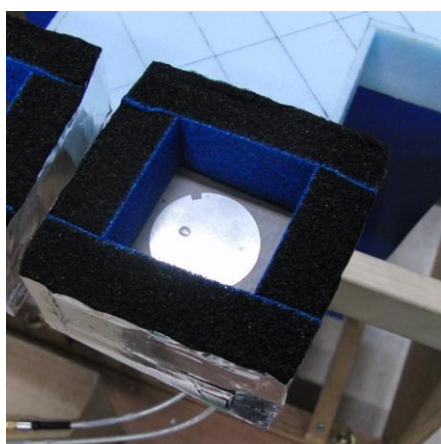

Figure5.2 Picture of tracking antenna with radio wave absorbers

And the distance between two antennas d_1 was set to 122mm (=λ). By this change, the incident angle between -14.5deg. to +14.5deg. has come to be detected.

In addition, the phase comparator "Arumo Tech – FS00T2703" (Figure5.3) is installed in the tracking system. This device has two RF input ports and one DC output port. The DC signal is output from the port in response to the phase difference of two input microwave. The internal circuit of this phase comparator is shown in Figure5.4. The microwaves which is come from input ports are amplified +60dB by log amplifiers to uniform the amplitude of two signals. It is because the powers of each input wanes have individual differences which are derive from the individual difference of tracking antenna's polarization shape as explained in Section3.5.2. Then two input signals are combined at the mixer and normalized at the operational amplifier. The connector shape of input port and output port is BNC-J, but input ports have to be SMA-J. So the BNC-J/SMA-J conversion connectors are installed at each input port. The specification of this phase comparator is follow; the frequency range is from 2.3GHz to 2.5GHz, the detectable phase difference is from 10deg. to 170deg., and the power range of input signal is from -60dBm to -10dBm.
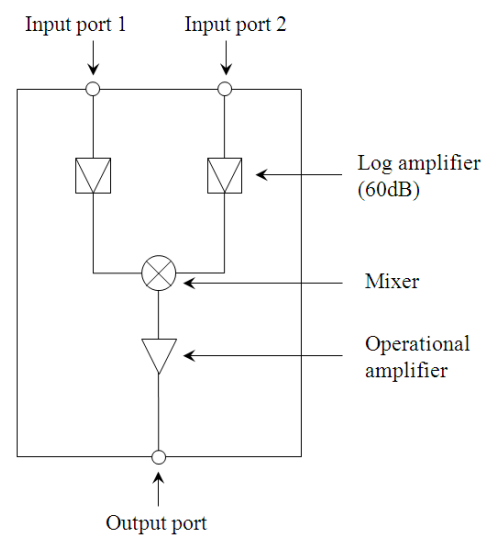
Figure5.3 Picture of phase comparator (Left)

Figure5.4 Internal circuit of phase comparator (Right)

Using this phase comparators, the tracking system is restructured as shown in Figure 5.5.

Pilot signal
(2.45GHz)

α

$d_1\sin\alpha$

Tracking antenna

d_1

$+\pi/2$ phase shifter

Log amplifier
(60dB)

Phase comparator

Mixer

Detector

V_{out1}

V_{out2}

PC

BNC connector box

$d=110\text{mm}$

d_1

$d_1=122\text{mm}$
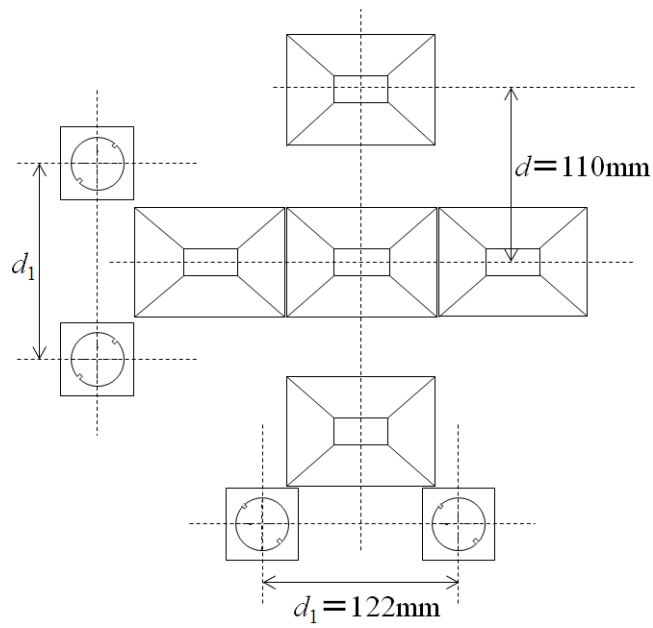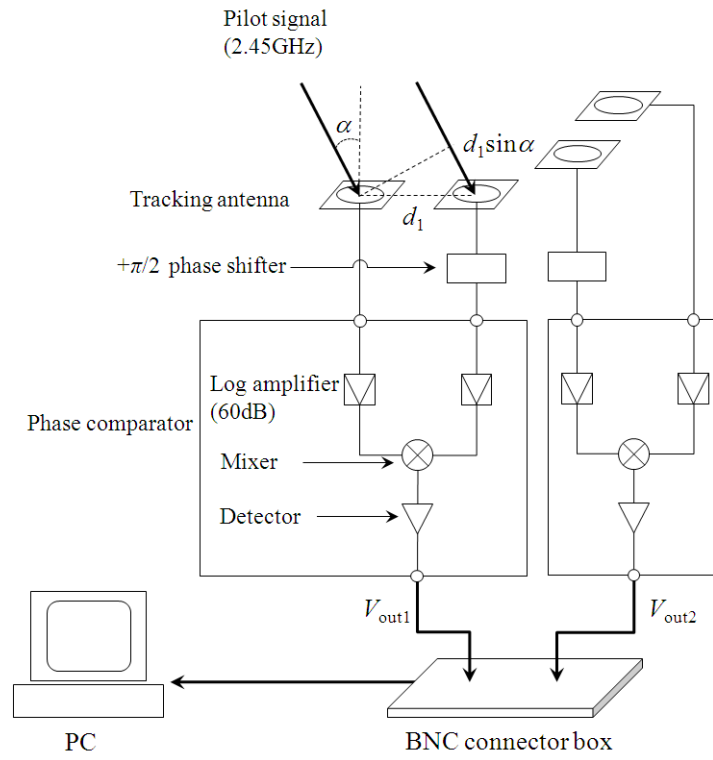
Figure5.5 Diagram of 2D tracking system with phase comparators

In the same way as Section3.5.1, the relationship between the incident angles of pilot signal α and the output voltage V_{out} was decided as follows.

$$V_{\text{out}} = \eta_1 + \eta_2 \sin(kd \sin \alpha) \tag{5.1}$$

Here η_1 and η_2 are fitting coefficients. The value of η_1 and η_2 were calculated from the measurement result which is shown in Figure 5.6. The measurement set up is almost same as Figure3.18, but the pilot-signal transmitting antenna is set at height of 1500mm. From these results, the fitting coefficients η_1 and η_2, η_3 and η_4 are decided as

x-direction: $\eta_1 = 0.93$, $\eta_2 = -0.76$

y-direction: $\eta_3 = 0.91$, $\eta_4 = -0.78$
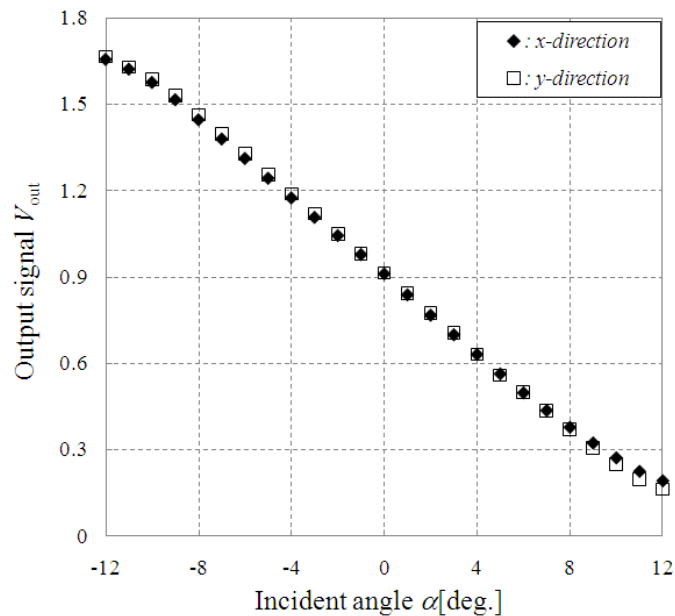
Figure5.6 Relationship between incident angles and output voltage

In the same way as Section3.5.2, the demonstration test of 2D tracking is done. The pilot-signal transmitting antenna with the 2.45GHz oscillator is attached at the rotation equipment which is constructed from a supporting bar and an electrical motor. And they are set at the altitude of 1500mm and the rotation radius was 237mm which are corresponding incident angle was 9.0deg.. The rotation period was 1.62second per round. That is, the rotation speed was 37.0rpm. Figure5.7 shows the estimated incident angles using the correlation shown in Figure5.6, and the estimated positions are plotted in Figure5.8.

46

In the same way as Section3.5.3, the error between the estimated position and actual position of the MAV model are calculated. Figure5.9 shows the error of radial-direction α_{rad} and Figure5.10 shows the error of azimuth-direction α_{azi}. As will be find from Figure5.9, the error of α_{rad}, is oscillating between about -1.5deg. to about 0.5deg. The maximum error is -1.79deg. (absolute value is 1.79deg.) Given that the 5.8GHz transmitting beam divergence is 9deg., the error 1.79deg. is sufficiently small. And then, from Figure5.10, the error of α_{azi} is oscillating between about -2deg. to about 0.5deg. The maximum error is -1.97deg. (absolute value is 1.97deg.) This value is sufficiently small, too.
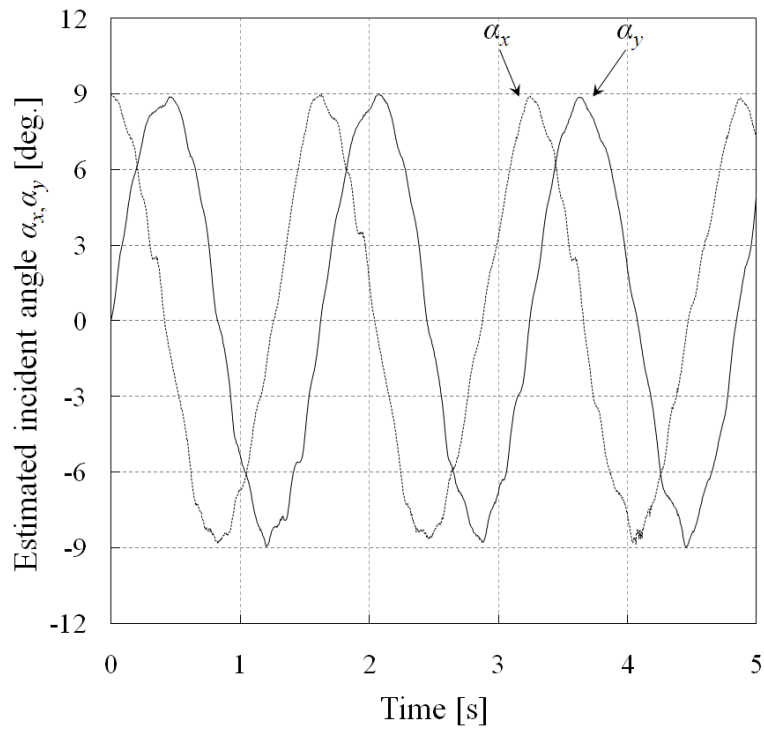

Figure5.7 Estimated incident angles α_x and α_y while the MAV model is circling at the radius of 237mm and the altitude of 1500mm with phase comparators
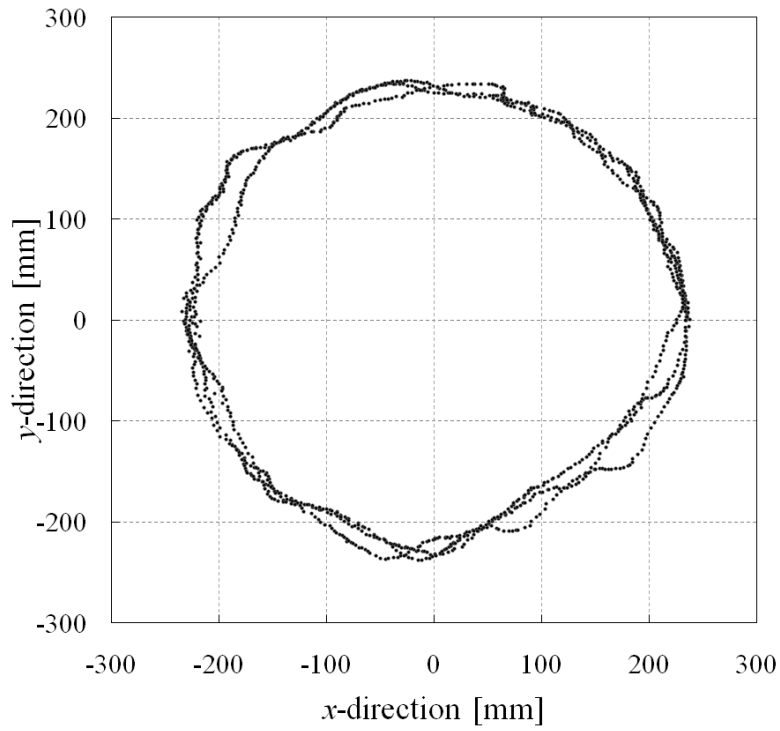
Figure5.8 Estimated position of the MAV model with phase comparators
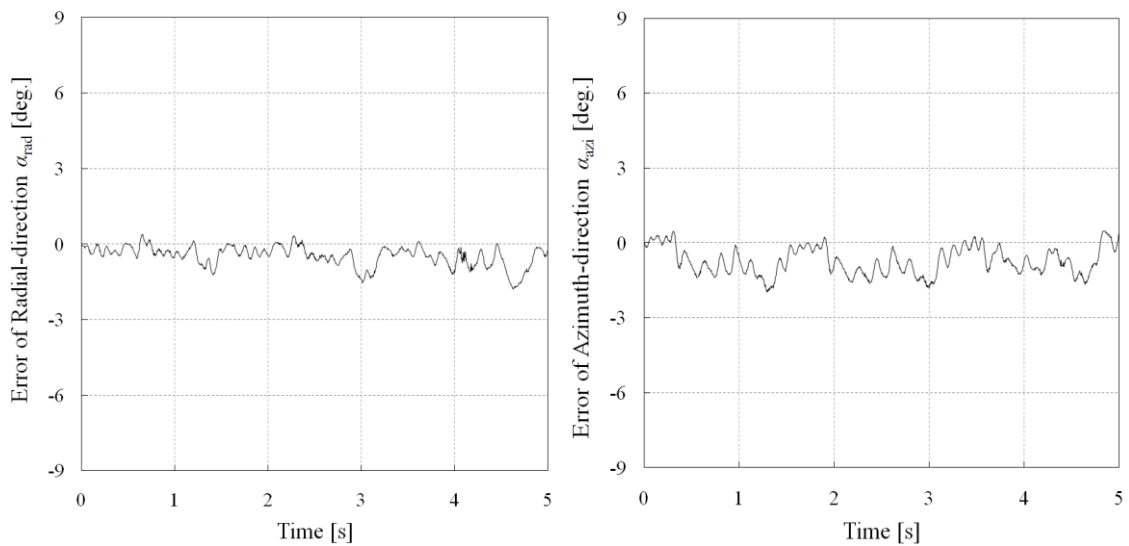
Figure5.9 Error of Radial-direction α_{rad} with phase comparators (Left)

Figure5.10 Error of azimuth-direction α_{azi} with phase comparators (Right)

Figure5.11 shows the total ground system of MWPT developed in our laboratory. As will be find from this figure, the total system is very compact. It is because the theories of phased array and retro-directive are simple. And LabVIEW programs of transmitting system and tracking system are integrated as shown in Figure5.12. The computing time of this program is about 79ms.
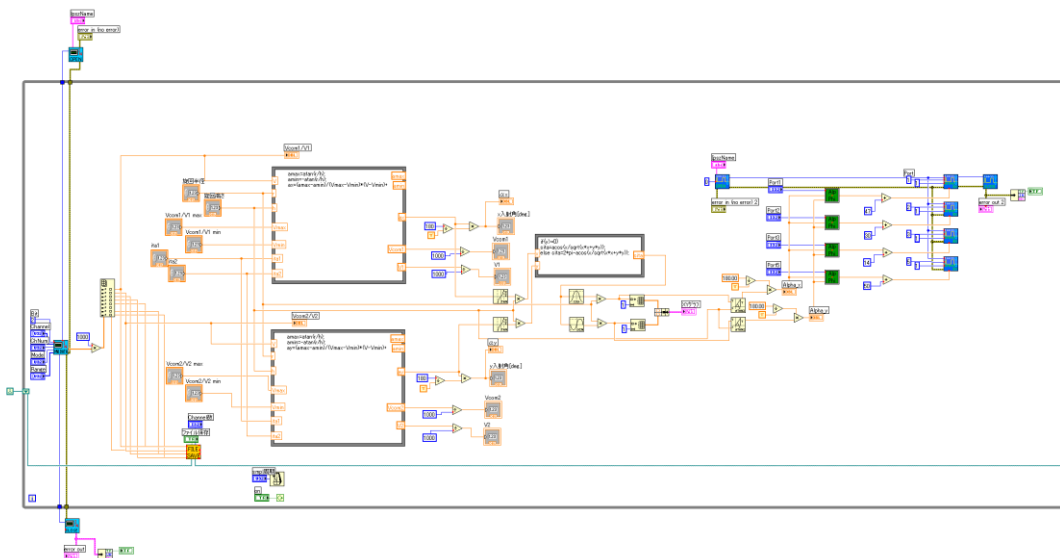

Figure5.12 LabVIEW program of auto-tracking phased array system
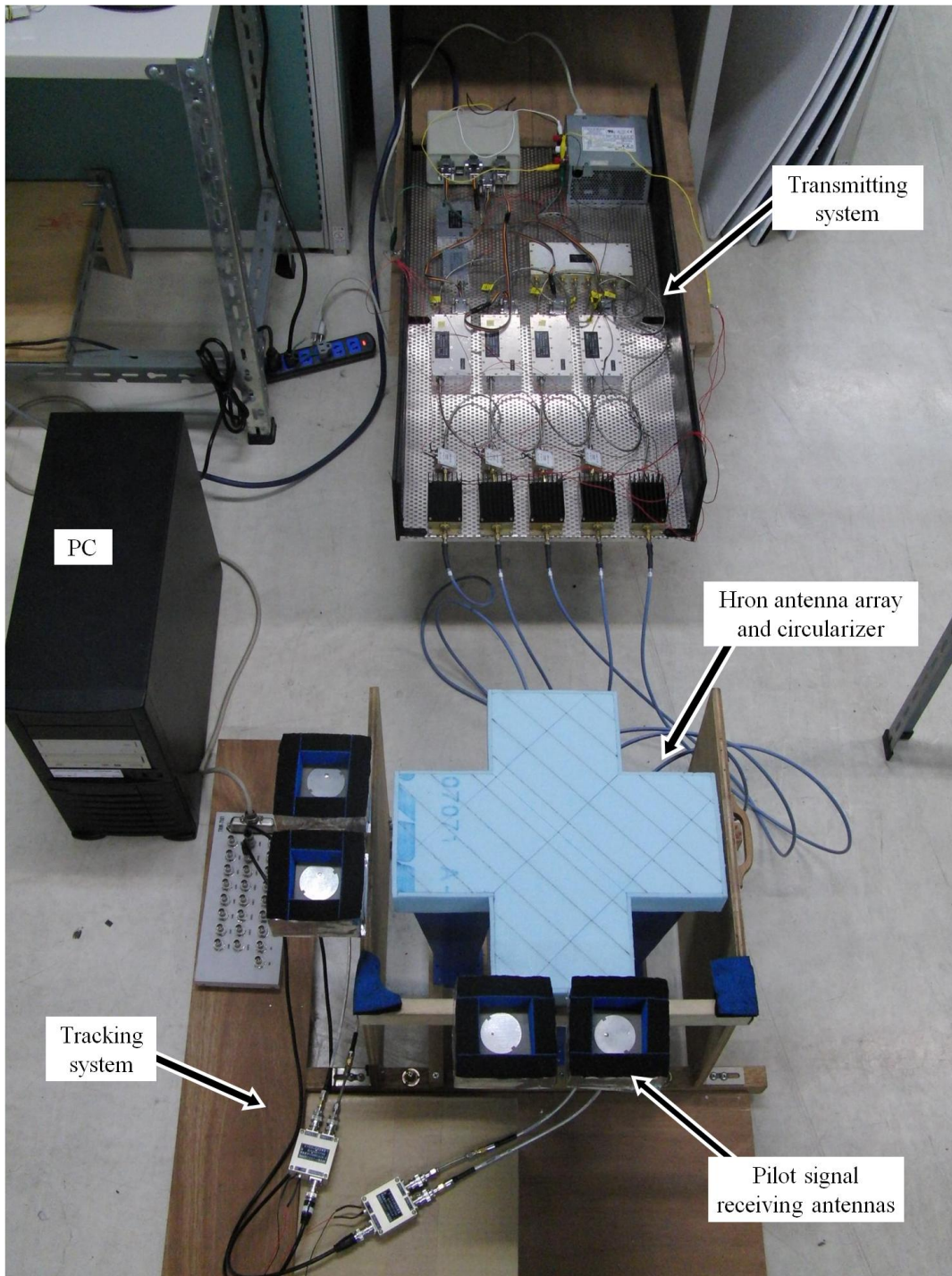
Figure5.11 Picture of total ground system of MWPT

5.2 Demonstration

5.2.1 Demonstration overview

With the three systems, transmitting system, tracking system, and receiving system, the demonstration of auto-tracking wireless power transmission is done. The overview of demonstration is following. First, the MAV model which is circling over the ground system radiates the 2.45GHz pilot signal. And next, the tracking antennas receive that signal and the PC calculates and detects the MAV position. And then, the PC sends the beam pointing information to the transmitting system and the transmitting system steer the microwave beam toward the MAV. At last, the MAV model receives the microwave beam and the electrical small motor with propeller which is attached on the MAV model is rotated by receiving power.

5.2.2 Demonstration setup

The experimental set up is shown in Figure5.13. The MAV model was circling using a motor and a supporting bar. They are set at the altitude of 1500mm and the rotation radius was 237mm which are corresponding incident angle was 9deg.. The pilot-signal transmitting antenna and 10elements of the rectennas are attached on the MAV model as shown in Figure5.14.

51
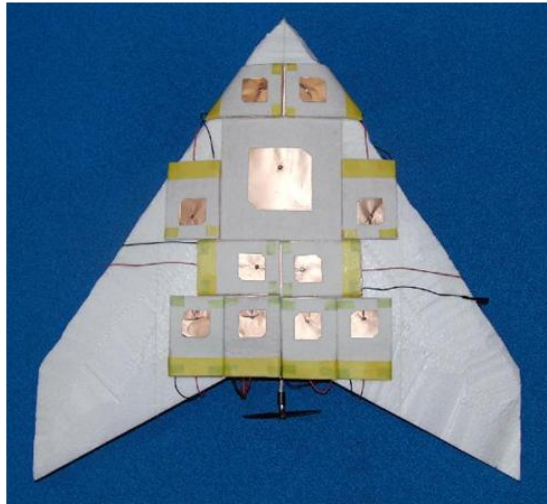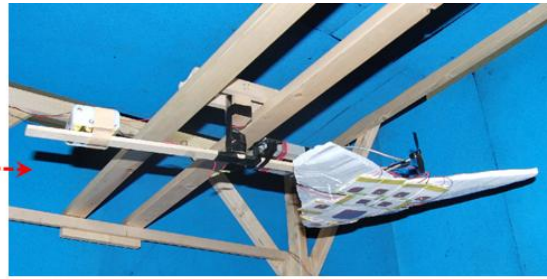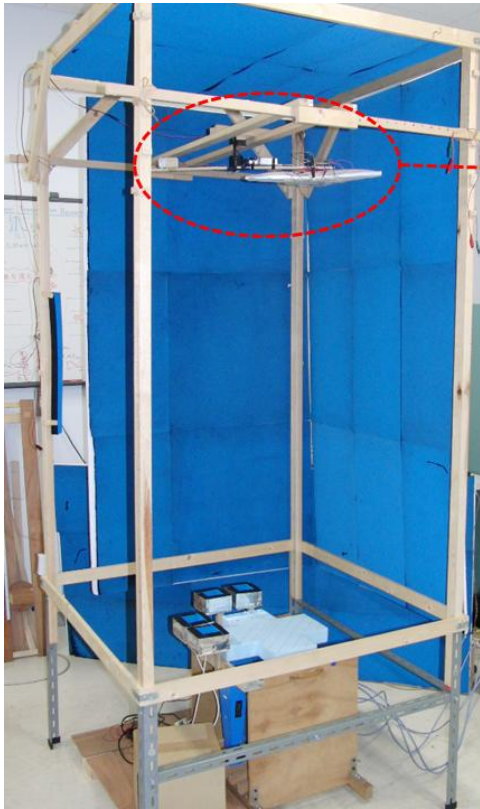
Figure5.13 Picture of demonstration set up (Left)

Figure5.14 Picture of MAV model (Right)

10elements of rectennas are parallel-connected, so matched road resistance of this rectenna array is 10Ω. Because of the internal resistance of the electrical small motor is about 4Ω, rectification efficiency of rectenna array is higher than that of one element of rectenna. Fugure5.15 shows the picture of the electrical small motor and Table5.1 shows the specification.
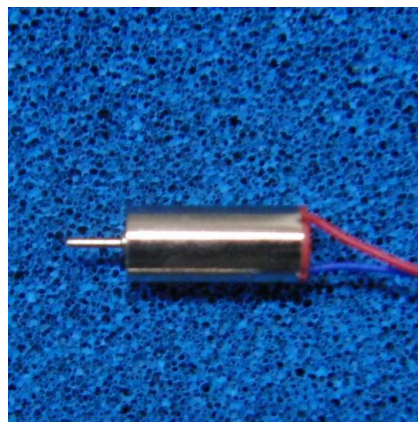
Figure5.15 Picture of electrical small motor

Table5.1 Specification of electrical small motor

| Minimum operating voltage [V]	0.1
Minimum operating current [A]	0.01
Inertial resistance [Ω]	4

5.2.3 Result of demonstration

The demonstration became successful. The electrical small motor with propeller rotates at each yaw angle. The propeller rotation is stable and fast.

5.3 Receiving power measurement

From demonstration result, the power how much the MAV model receives is measured. To measure the receiving power, the variable resistance (Figure5.16) is used for impedance matching as the road resistance and the voltage between both ends of the resistance is measured by using the digital multi-meter (Figure5.17). In this measurement, two different values of resistance, 4Ω and 10Ω, are used. The MAV circling angle θ is defined as Figure5.18 shown and the receiving power is measured at every 15deg..

Figure5.19 shows the result of 4Ω. As will be find from this figure, the receiving power is nearly constant at any circling angle, and the average power is about 9.8mW. And the rectenna array can receive 8mW constantly. Considering that the minimum operating power of the electrical small motor is about 1mW, the rectenna array can receive enough power to rotate the propeller. But there is a little variation. It is because the circularizer and the rectenna have polarizations whose shape is not pure circle. So the receiving power of antennas may change at each circling angle and rectifier efficiency which depends on input power change at each point. In addition, the accuracy of tracking system is not perfect, so the tracking performance is one of the causes of the variation.

Figure5.20 shows the result at 10Ω. Comparing Figure5.20 with Figure5.19, the receiving power using 10Ω resistance is higher than that of 4Ω resistance. The average power is about 13.1mW. It is because the 10Ω is the matching impedance of the road resistance. But there is variation and the reasons of this are same as 4Ω.

53

Figure5.16 Picture of variable resistance

Figure5.17 Picture of digital multi-meter
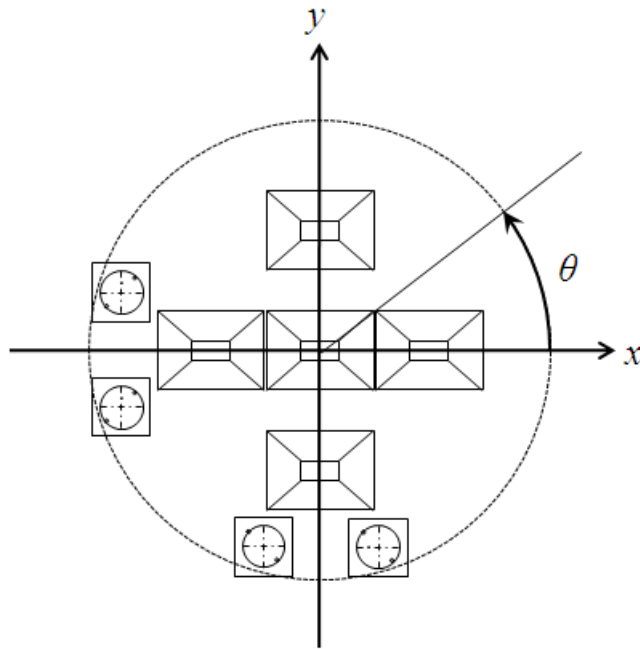
Figure5.18 Description of circling angle
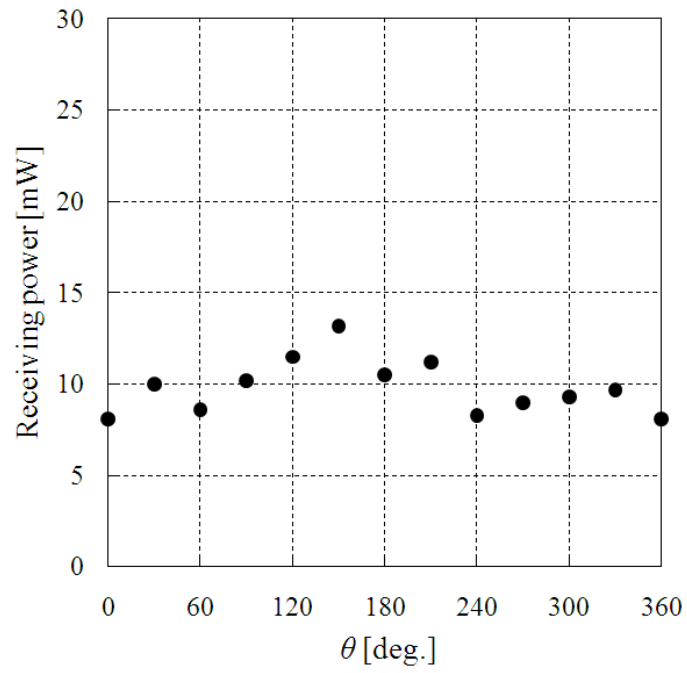
Figure5.19 Receiving power at 4Ω
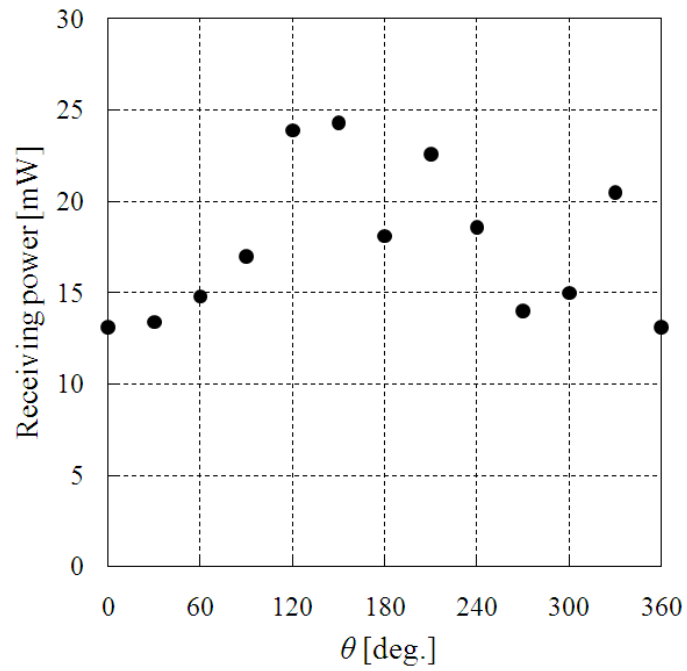
Figure5.20 Receiving power at 10Ω

Chapter 6.   Conclusions

At the transmitting system, the ideal Gaussian beam can be formed using the active phased array antenna. And it can be steered by shifting the microwave phase.

At the tracking system, the 2D tracking became successful by using the software retro-directive function. And the error of the tracking system is sufficiently small considering the divergence angle of transmitting beam.

At the receiving system, the light-weight flexible patch rectenna array is developed.

The ground system specification

Transmitting system		Tracking system	
Parameters	Values	Parameters	Values
Microwave frequency f	5.8GHz	Microwave frequency f	2.45GHz
Wavelength λ	51.7mm	Wavelength λ	122.4mm
Total transmission power	5W	Pilot signal power	10mW
Horn array pitch d	110mm ($d/\lambda=2$)	Patch antenna pitch d_1	122.4mm ($\lambda/d=1$)
Beam steering angle θ_{ste}	9deg.	Detectable incident angle α	14.5deg.

The aerial system specification

Receiving system	
Parameters	Values
Microwave frequency f	5.8GHz
Rectenna type	Light-weight flexible patch
Polarization	Circular-polarized
Matching impedance	100Ω
Material	Felt pad, cupper tape

At the demonstration, the electrical small motor can be rotated by Auto-tracking Wireless Power Transmission.

The demonstration condition

Parameters	Values
Altitude	1500mm
Rotation radius	237mm
Number of rectenna	10
Operating power of motor	1mW
Mximum receiving power	24mW (10Ω resistance)

The receiving power is following.

4Ω : Maximum 13.2mW,   Minimum 8.0mW,   Average 9.8mW.

  →   Enough power to rotate the motor. (Minimum operating power is 1mW.)

10Ω : Maximum 24.3mW,   Minimum 13.1mW,   Average 17.6mW.

Reference

[1] Takayuki S., Yutaka A., Mnanobu O., Takaharu I., and Tadashi H. "Micowave Energy Transmission System for Microrobot", IEICE Trans. ELECTRON., VOL.E80-C, No.2 Feb. (1997)

[2] André Kurs, Aristeidis Karalis, Robert Moffatt, J. D. Joannopoulos, Peter Fisher, and Marin Soljačić, "Wireless Power Transfer via Strongly Coupled Magnetic Resonances", Science, 317 (5834), 83-86 (2007)

[3] 三菱総合研究所,『2005 年度宇宙航空研究開発機構委託業務成果報告書　宇宙エネルギー利用システム総合研究』

[4] Tesla N., "The transmission of electric energy without wires, The thirteenth Anniversary Number of the Electrical World and Engineer", March 5, 1904

[5] Brown, W.C.; "The history of power transmission by radio waves", IEEE Trans. MTT, 32 (9), 1230-1242 (1984)

[6] Komatsu S., Katsunaga K., Ozawa R., Komurasaki K., and Arakawa Y.: Power Transmission to a Micro Aerial Vehicle, AIAA paper 2007-1003 (2007)

[7] Kotajima.H, Kawamura.K, "Electrical Design of a Metal Grid Circularizer", Technical report of IEICE, RCS 98(600), 87-92, 1999-02-17.

[8] Ozawa R., "Development of Microwave Energy Supply System", Master thesis, The University of Tokyo, 2007.

[9] 嶋根愛理,『マイクロ波ソフトウェアリトロディレクティブ追尾システムとその高度化の研究』, 修士論文, 東京大学, 2009 年 3 月

[10] 岡田文明, 『マイクロ波工学　基礎と応用』, 山海堂, 2004.

[11] 電子情報通信学会, 『アンテナ工学ハンドブック』, オーム社, 1980.

[12] 後藤尚久, 『アンテナ工学入門講座』, 電波新聞社, 2008.

[13] 内藤喜之, 『マイクロ波・ミリ波工学』, コロナ社, 1986.

[14] Kuwano H., "Trends of Energy Harvesting Technologies", CMC Publishing Co., Ltd, 2010.

[15] Matsuki H., "Frontier of wirelesses Electric Power Transmission", CMC Publishing Co., Ltd, 2009.

[16] David M. Pozar, "MICROWAVE ENGINEERING", John Wiley & Sons, Inc., 2005.